Heliyon 7 (2021) e07592

Contents lists available at ScienceDirect

Heliyon

journal homepage: www.cell.com/heliyon

Research article

Design, synthesis, characterization, and antioxidant activity studies of novel thienyl-pyrazoles

Karthik Kumara [a,b], Malledevarapura Gurumurthy Prabhudeva [c], Channa Basappa Vagish [c], Hamse Kameshwar Vivek [d], Kuriya Madavu Lokanatha Rai [e], Neratur Krishnappagowda Lokanath [a,**], Kariyappa Ajay Kumar [c,*]

[a] Department of Studies in Physics, University of Mysore, Mysuru 570006, India
[b] Department of Physics, School of Sciences, Jain (Deemed to be) University, Bengaluru, 560 011, India
[c] Department of Chemistry, Yuvaraja College, University of Mysore, Mysuru 570005, India
[d] Faculty of Natural Sciences, Adichunchanagiri University-Center for Research and Innovation, Adichunchanagiri University, B.G. Nagara, Mandya, 571448, India
[e] Department of Studies in Chemistry, University of Mysore, Mysuru, 570006, India

ARTICLE INFO

Keywords:
Amberlyst-15
Annulation
Antioxidant
Hydroxyl
Chalcone
Docking

ABSTRACT

In a sustained search for novel and effective antioxidants, a potential therapeutic leads against renal, and neurological disorders. Amongst the heterocycles, pyrazole and their derivatives have been extensively studied for their biological potencies, particularly to a larger extent for their antioxidant properties. Although many of pyrazole derivatives displayed antioxidant activities, still there is a need of developing efficient protocol for their synthesis, involving ecofriendly conditions, molecules of greater antioxidant efficacy and lesser toxicity, etc. In this context, the current study presents an amberlyst-15 catalysed efficient synthesis of 2-pyrazoline derivatives, **5(a-g)** via (3 + 2) annulation of chalcones with phenylhydrazines. Structure proofs of new pyrazoles offered by spectral studies, and the molecular structure of compound **5d** of the series by crystallographic studies, which revealed an intra molecular hydrogen bond interactions (C–H···N type), and stabilization by C–H...π and π—π molecular interactions. Of the series, compounds **5g** and **5h** show excellent DPPH (IC_{50} = 0.245 ± 0.01, and 0.284 ± 0.02 μM); and hydroxyl (IC_{50} = 0.905 ± 0.01, and 0.892 ± 0.01μM) radical scavenging activities comparable with respective controls, ascorbic acid (IC_{50} = 0.483 ± 0.01μM) and BHA (IC_{50} = 1.739 ± 0.01μM). The molecular docking and ADME/Tox studies indicate that, these compounds have good antioxidant activity through π-π stacking with Catalase *via* Try337 and Phe140, and therefore, might be lead antioxidants for further study.

1. Introduction

Oxidative stress induced by the free radical damage cell membranes, and nucleic acids, which results in aging, cancer, atherosclerosis, and Alzheimer's disease [1]. The studies on small-molecules with antioxidant efficacy to prevent the deleterious effects is important field of research. The drug molecules that contains a pyrazole core remain as choice in medicinal chemistry towards more practical antioxidant agents [2]. The pyrazole derivatives were prepared in good to excellent chemical yields by the silver chloride catalyzed isomerization of *α*, *β*-acetylenic hydrazones in dichloromethane at room temperature [3]. The molecular iodine catalyzed reaction of α,β-unsaturated ketones and sulfonyl hydrazide [4], the four-component reaction of dialkyl acetylenedicarboxylates, isocyanides, ethyl acetoacetate and hydrazine/phenylhydrazine produce pyrazoles [5], The (3 + 2) annulation of chalcones with thiosemicarbazide [6], and hydrazines with ynone trifluoroborates [7] gave pyrazoles with regioselectivity. The Chloramine-T catalyzed 1,3-dipolar cycloaddition of hydrazones to alkenes form pyrazoles [8].

Several natural and synthetic pyrazole derivatives possess wide spectrum of pharmacological potentials with druggable properties [9]. For instance, the pyrazole analogs exhibit cytotoxicity against DLA cells, reduces tumour loads, and downregulates tumour progression proliferation [10]. The pyrazole derivatives have antidiabetic and anti-inflammatory [11], antimicrobial [12], and acetylcholinesterase inhibitor [13] properties. The Salvia officinalis L belongs to Lamiaceae family is known for its antioxidant and many pharmaceutical potencies,

* Corresponding author.
** Corresponding author.
E-mail addresses: lokanath@physics.uni-mysore.ac.in (N.K. Lokanath), ajaykumar@ycm.uni-mysore.ac.in (K. Ajay Kumar).

https://doi.org/10.1016/j.heliyon.2021.e07592
Received 17 April 2021; Received in revised form 19 June 2021; Accepted 13 July 2021

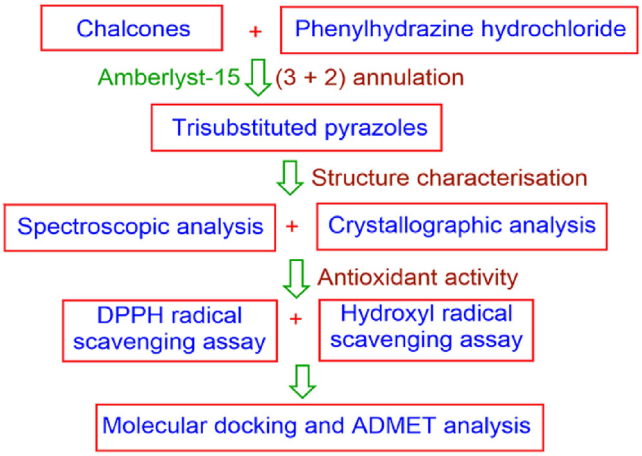

Figure 1. The research methodology flowchart.

like anti-spasmodic, astringent, sedative, anti-hyperglycemic, and anti-inflammatory [14]. The complexes isolated from Black Sea marine inverterbrate tissues have displayed antioxidant, antimicrobial and mitogenic activities [15]. Main protease (Mpro) in the life cycle of SARS-CoV-2 mediate viral replication, transcription, and is a drug target for the virus, the computational results reveal a hypothesis for experimental validation [16].

The pyrazole motif is an important core in the development of antioxidants, that alone or combined with other pharmacophore shows high degree of antioxidant activity [17]. For instance, the *N*-formyl pyrazolines synthesized via Michael addition displayedd promising anticancer and antioxidant [18], and pyrazolo-pyrimidines possess cytotoxic and radical scavenging properties [19]. The reports on the curcumin pyrazole analogs indicated that these alleviate oxidative stress-induced PC12 neuronal damage abilities [20], and pyrazole-thiazoles show antimicrobial and antioxidant activities [21]. The prepared pyrazole-triazole hybrids displayed citotoxic and antioxidant [22], and pyrazole aldehydes have xanthine oxidase inhibitory [23] properties.

Although, a plenty of research on pyrazoles and their biological activities has been reported. Many of the methods adopted for the synthesis requires drastic reaction conditions, and produces less yields, and more toxic bi-products, etc. Furthermore, the most of the pyrazole derivatives exhibited lesser antioxidant properties comparable with the standards employed. In this context, in an attempt towards new therapeutics with greater antioxidant potentials and less toxicity, and to overcome drawbacks of synthetic procedure, the present work has been undertaken. The current study demonstrates the Amberlyst-15 catalyzed reaction of

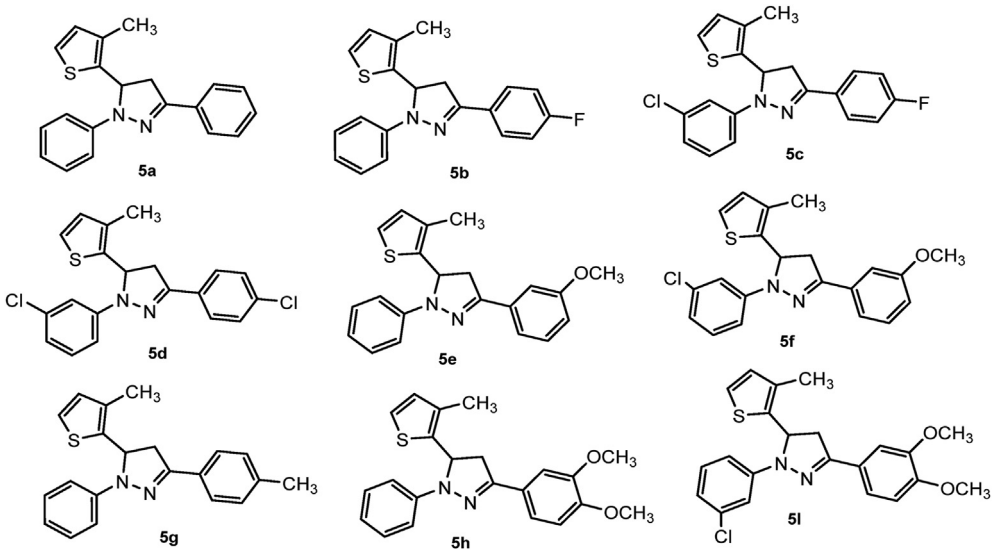

Figure 2. The chemical structures of the synthesized compounds **5(a-i)**.

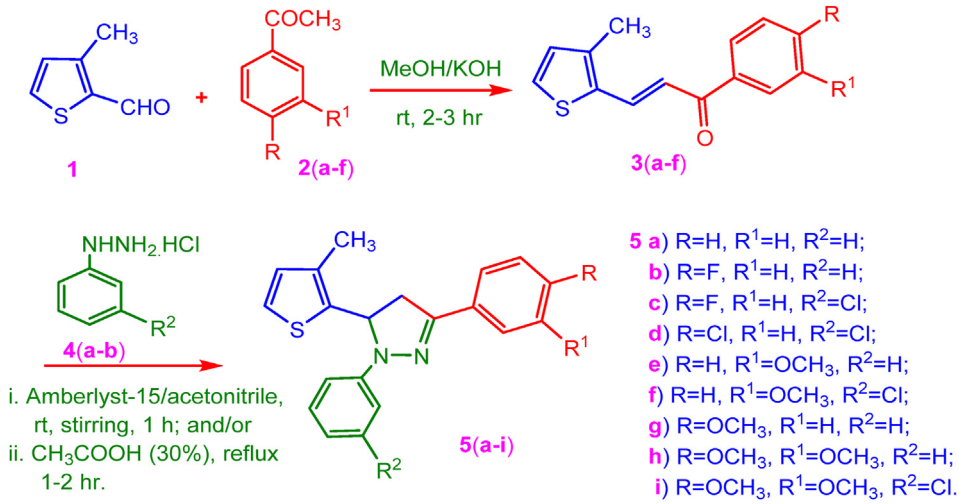

Figure 3. Synthetic route for thienyl-pyrazolines **5(a-i)**.

Table 1. Reaction time and yields of Amberlyst-15 mediated and conventional synthesis.

Compound	Amberlyst-15 mediated method		Conventional Method		Melting Point (°C)
	Time (Min)	Yield (%)	Time (Min)	Yield (%)	
5a	52	72	75	68	96–98
5b	47	67	75	61	102–103
5c	54	78	115	70	102–104
5d	50	88	85	79	116–117
5e	56	77	110	69	110–112
5f	57	70	105	63	120–122
5g	45	76	65	71	94–96
5h	45	79	70	70	119–121
5i	60	78	120	72	149–151

chalcones, and phenylhydrazine hydrochlorides at room temperature to get thienyl-pyrazoles in good yields. The structures of synthesized compounds were characterized through spectral analysis, and one compound by crystallographic studies. After the structural characterization, the new compounds were assessed for free radical scavenging activities. Furthermore, an *in silico* molecular docking and ADMET analysis was carried out to validate the results and their mode of action.

2. Experimental

2.1. Materials and methods

All the chemicals and reagents procured from Sigma Aldrich were used as received. Pre-coated silica gel-aluminum plates (Merck, F-254) used for thin-layer chromatography (TLC). IR Spectra were obtained on PerkinElmer FT-IR Spectrophotometer, ^{1}H NMR (400 MHz) and ^{13}C NMR (100 MHz) spectra were obtained on Agilent NMR spectrometer. Mass spectra were obtained on Lynx SCN781 spectrometer (TOF mode). Absorbance was recorded on ELICO SL 159 UV-Vis spectrophotometer. The un-corrected melting points were with Centex apparatus.

Table 2. Crystal structure data and refinement details of molecule **5d**.

Parameter	value
CCDC deposit No.	1838509
Empirical formula	$C_{20}H_{16}N_2SCl_2$
Formula weight	387.32
Temperature	293 K
Wavelength	0.71073 Å
Crystal system, space group	Monoclinic, $P2_1/a$
Unit cell dimensions	$a = 17.840(5)$ Å
	$b = 5.779(4)$ Å
	$c = 19.270(7)$ Å
	$\alpha = 90^\circ$ $\beta = 112.20(2)^\circ$ $\gamma = 90^\circ$
Volume	1839.4(2) Å^3
Z	4
Density(calculated)	1.399 Mg m $^{-3}$
Absorption coefficient	0.471 mm $^{-1}$
F_{000}	800
Crystal size	0.27 × 0.24 × 0.21 mm
θ range for data collection	3.38° - 27.57°
Index ranges	$-16 \leq h \leq 23$
	$-3 \leq k \leq 7$
	$-24 \leq l \leq 25$
Reflections collected	6493
Independent reflections	4133 [$R_{int} = 0.0921$]
Absorption correction	multi-scan
Refinement method	Full matrix least-squares on F^2
Data/restraints/parameters	4133/0/227
Goodness-of-fit on F^2	1.001
Final [I > 2σ(I)]	$R1 = 0.0778$, $wR2 = 0.1763$
R indices (all data)	$R1 = 0.1873$, $wR2 = 0.2338$
Largest diff. peak and hole	0.272 and −0.304 e Å $^{-3}$

2.2. Synthesis of thienyl-pyrazoles, 5(a-i)

A mixture of chalcones, **3**(**a-f**) (5 mmol), phenylhydrazine hydrochlorides, **4**(**a-b**) (5 mmol), and Amberlyst-15 (10%, w/w) in acetonitrile (25 mL) was stirred at room temperature for 30–60 min. After the completion, the separated solid was filtered, washed with diethyl ether (2 × 20 mL), then treated with ethyl acetate (20 mL), and stirred for 10 min and again filtered. The filtrate was concentrated under vacuum, the solid formed was triturated in diethyl ether, filtered and dried to get the products **5**(**a-i**). Alternatively, the reaction was carried out in 30% acetic acid under boiling conditions.

2.2.1. 5-(3-Methylthiophen-2-yl)-1,3-diphenyl-4,5-dihydro-1H-pyrazole, 5a

Obtained from 3-(3-methylthiophen-2-yl)-1-phenylprop-2-en-1-one, **3a** (1.14g, 5 mmol) and phenylhydrazine hydrochloride, **4a** (0.72g, 5 mmol); ^{1}H NMR ($CDCl_3$, δ ppm): 2.665 (s, 3H, CH_3), 3.004–3.064 (dd, 1H, $J = 6.8, 16.8$Hz, C_4-H_a), 3.731–3.803 (dd, 1H, $J = 12.4$ 17.2Hz, C_4-H_b), 5.190–5.237 (dd, 1H, $J = 6.4, 12.4$ Hz, C_5–H), 6.70–6.818 (m, 5H, Ar–H), 6.998–7.063 (m, 4H, Ar–H), 7.208–7.245 (m, 3H, Ar–H); ^{13}C NMR ($CDCl_3$, δ ppm): 16.49 (1C, CH_3), 43.661 (1C, C-4), 64.37 (1C, C-5), 105.14 (1C), 111.25 (1C), 119.14 (1C), 123.44 (1C), 125.33 (1C), 125.70 (1C), 126.071 (1C), 126.53 (1C), 127.58 (1C), 128.42 (1C), 128.72 (1C), 129.30 (1C), 129.84 (1C), 134.92 (1C), 141.40 (1C), 142.96 (1C), 145.23 (1C, C-3). MS (m/z): 318.0 (M+, 100); Anal. Calcd. (found) for $C_{20}H_{18}N_2S$ (%): C, 75.44 (75.32); H, 5.70 (5.67); N, 8.80 (8.75).

2.2.2. 3-(4-Fluorophenyl)-5-(3-methylthiophen-2-yl)-1-phenyl-4,5-dihydro-1H-pyrazole, 5b

Obtained from 1-(4-fluorophenyl)-3-(3-methylthiophen-2-yl)prop-2-en-1-one, **3b** (1.23g, 5 mmol) and phenylhydrazine hydrochloride, **4a** (0.72g, 5 mmol); ^{1}H NMR ($CDCl_3$, δ ppm): 2.83 (s, 3H, CH_3), 3.01–3.069 (dd, 1H, $J = 6.8, 16.8$Hz, C_4-H_a), 3.737–3.810 (dd, 1H, $J = 12.4, 17.2$Hz, C_4-H_b), 5.197–5.245 (dd, 1H, $J = 6.8, 12.4$Hz, C_5–H), 6.619–6.890 (m, 2H, Ar–H), 7.001–7.068 (m, 5H, Ar–H), 7.152–7.248 (m, 4H, Ar–H); ^{13}C NMR ($CDCl_3$, δ ppm): 13.68 (1C, CH_3), 46.42 (1C, C-4), 63.72 (1C, C-5), 111.29 (1C), 113.56 (1C), 115.29 (1C), 116.26 (1C), 119.34 (1C), 121.96 (1C), 125.44 (1C), 126.08 (1C), 126.46 (1C), 127.47 (1C), 128.97 (1C), 129.87 (1C), 130.29 (1C), 130.46 (1C), 131.13 (1C), 131.80 (1C), 143.16 (1C), 163.51 (1C, C-3). MS (m/z): 336.0 (M+, 100); Anal. Calcd. (found) for $C_{20}H_{17}FN_2S$ (%): C, 71.40 (71.34); H, 5.05 (5.09); N, 8.33 (8.28).

2.2.3. 1-(3-Chlorophenyl)-3-(4-fluorophenyl)-5-(3-methylthiophen-2-yl)-4,5-dihydro-1H-pyrazole, 5c

Obtained from 1-(4-fluorophenyl)-3-(3-methylthiophen-2-yl)prop-2-en-1-one, **3b** (1.23g, 5 mmol) and 3-chlorophenylhydrazine

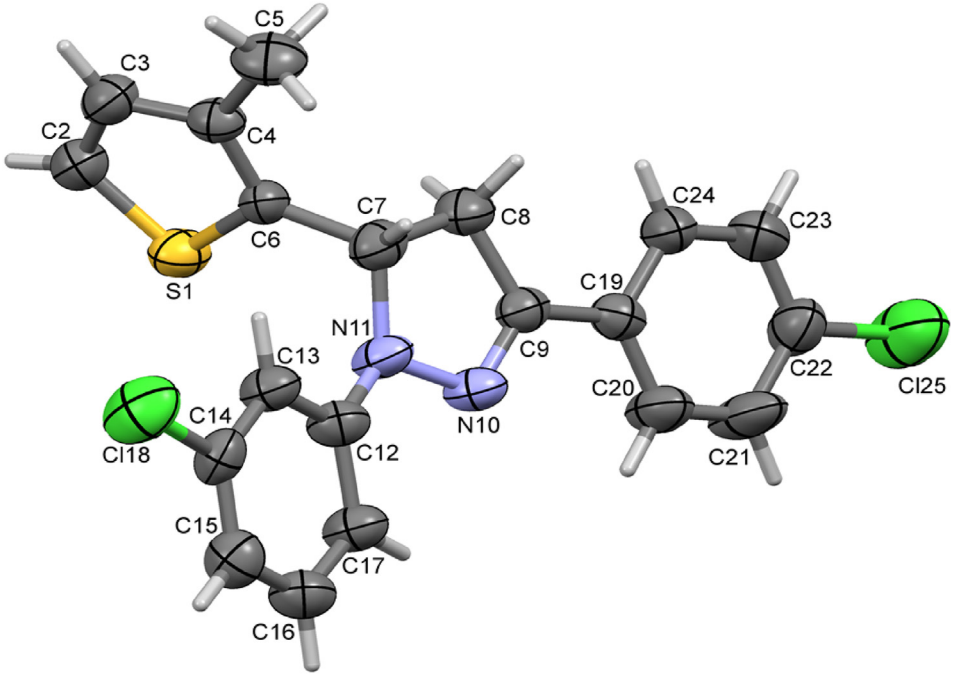

Figure 4. *ORTEP* of the compound **5d** with thermal ellipsoids drawn at 50% probability.

hydrochloride, **4b** (0.89g, 5 mmol); ^{1}H NMR ($CDCl_3$, δ ppm): 2.310 (s, 3H, CH_3), 3.014–3.073 (dd, 1H, *J* = *6.8,116.*8Hz, C_4-H_a), 3.713–3.786 (dd, 1H, *J* = *12.4, 17.*6Hz, C_4-H_b), 5.168–5.216 (dd, 1H, *J* = *6.8, 12.*0Hz, C_5–H), 6.699–6.809 (m, 4H, Ar–H), 6.995–7.249 (m, 6H, Ar–H); ^{13}C NMR ($CDCl_3$, δ ppm): 14.06 (1C, CH_3), 43.72 (1C, C-4), 64.18 (1C, C-5), 111.26 (1C), 113.51 (1C), 119.07 (1C), 125.27 (1C), 125.62 (1C), 126.43 (2C), 127.37 (1C), 128.55 (1C), 129.02 (1C), 129.41 (1C), 131.54 (1C), 134.87 (1C), 137.67 (1C), 138.45 (1C), 142.95 (1C), 145.28 (1C, C-3). MS (*m/z*): 370.1 (M+, 100), 372.14 (M+2, 33); Anal. Calcd. (found) for $C_{20}H_{16}ClFN_2S$ (%): C, 64.77 (64.74); H, 4.35 (4.32); N, 7.55 (7.51).

2.2.4. 1-(3-Chlorophenyl)-3-(4-chlorophenyl)-5-(3-methylthiophen-2-yl)-4,5-dihydro-1H-pyrazole, 5d

Obtained from 1-(4-chlorophenyl)-3-(3-methylthiophen-2-yl)prop-2-en-1-one, **3c** (1.31g, 5 mmol) and 3-chlorophenylhydrazine hydrochloride, **4b** (0.89g, 5 mmol); ^{1}H NMR ($CDCl_3$, δ ppm): 2.249 (s, 3H, CH_3), 2.940–2.998 (dd, 1H, *J* = *17.2, 6.*4Hz, C_4-H_a), 3.864–3.937 (dd, 1H, *J* = *12.0, 17.*2Hz, C_4-H_b), 5.497–5.543 (dd, 1H, *J* = *6.4, 12.*4Hz, C_5–H), 6.592–6.617 (m, 1H, Ar–H), 6.742–6.800 (m, 2H, Ar–H), 7.003–7.154 (m, 5H, Ar–H), 7.384–7.467 (m, 2H, Ar–H); ^{13}C NMR ($CDCl_3$, δ ppm): 13.78 (1C, CH_3), 42.18 (1C, C-4), 60.68 (1C, C-5), 101.35 (1C), 105.84 (1C), 108.14 (1C), 110.73 (1C), 113.20 (1C), 119.08 (1C), 120.52 (1C), 126.43 (1C), 128.08 (1C), 129.90 (1C), 132.44 (1C), 134.13 (1C), 134.99 (1C), 137.30 (1C), 145.27 (1C), 148.05 (1C), 148.73 (1C, C-3). MS (*m/z*): 390.0 (M+4, 10), 388.0 (M+2, 63), 386.0 (M+, 100); Anal. Calcd. (found) for $C_{20}H_{16}Cl_2N_2S$ (%): C, 62.02 (61.95); H, 4.16 (4.12); N, 7.23 (7.19).

2.2.5. 3-(3-Methoxyphenyl)-5-(3-methylthiophen-2-yl)-1-phenyl-4,5-dihydro-1H-pyrazole, 5e

Obtained from 1-(3-methoxyphenyl)-3-(3-methylthiophen-2-yl)prop-2-en-1-one, **3d** (1.27g, 5 mmol) and phenylhydrazine hydrochloride, **4a** (0.72g, 5 mmol); ^{1}H NMR ($CDCl_3$, δ ppm): 2.289 (s, 3H, CH_3), 3.323–3.368 (dd, 1H, *J* = *4.4, 5.*2Hz, C_4-H_a), 3.816 (s, 3H, OCH_3), 3.877–3.923 (dd, 1H, *J* = *11.6, 17.*2Hz, C_4-H_b), 5.696–5.736 (dd, 1H, *J* = *4.8, 12.*0Hz, C_5–H), 6.731 (s, 2H, Ar–H), 6.907–7.023 (m, 5H, Ar–H),

Table 3. Bond lengths (Å) of compound **5d**.

Atoms	XRD	DFT	Atoms	XRD	DFT
Cl18–C14	1.743(6)	1.764	C8–C9	1.506(8)	1.515
Cl25–C22	1.737(6)	1.757	C9–C19	1.461(8)	1.463
S1–C2	1.701(6)	1.733	C12–C13	1.400(8)	1.406
S1–C6	1.723(5)	1.751	C12–C17	1.397(8)	1.408
N10–N11	1.414(5)	1.371	C13–C14	1.371(8)	1.393
N10–C9	1.295(7)	1.292	C14–C15	1.363(8)	1.391
N11–C7	1.477(7)	1.488	C15–C16	1.394(8)	1.397
N11–C12	1.390(7)	1.401	C16–C17	1.378(8)	1.389
C2–C3	1.370(8)	1.364	C19–C20	1.385(8)	1.409
C3–C4	1.413(8)	1.436	C19–C24	1.383(7)	1.405
C4–C5	1.503(8)	1.507	C20–C21	1.382(9)	1.388
C4–C6	1.371(8)	1.377	C21–C22	1.374(9)	1.398
C6–C7	1.497(8)	1.505	C22–C23	1.347(8)	1.392
C7–C8	1.553(8)	1.556	C23–C24	1.383(9)	1.394
Correlation Coefficient (CC)					0.9929

Table 4. Bond angles (°) of compound **5d**.

Atoms	XRD	DFT	Atoms	XRD	DFT
C2–S1–C6	91.8(3)	91.4	N11–C12–C13	121.0(5)	120.2
N11–N10–C9	108.4(4)	110.3	N11–C12–C17	120.1(5)	120.6
N10–N11–C7	112.0(4)	112.3	C13–C12–C17	118.8(5)	119.3
N10–N11–C12	118.2(4)	118.6	C12–C13–C14	119.9(5)	119.1
C7–N11–C12	123.8(4)	124.1	Cl18–C14–C13	118.6(4)	118.3
S1–C2–C3	111.5(4)	111.7	Cl18–C14–C15	119.2(4)	119.2
C2–C3–C4	113.3(5)	113.6	C13–C14–C15	122.2(5)	122.4
C3–C4–C5	123.5(5)	122.2	C14–C15–C16	118.3(5)	117.7
C3–C4–C6	111.5(5)	111.8	C15–C16–C17	121.3(5)	121.6
C5–C4–C6	124.9(5)	126	C12–C17–C16	119.7(5)	119.9
S1–C6–C4	111.8(4)	111.6	C9–C19–C20	122.2(5)	121
S1–C6–C7	119.7(4)	119.9	C9–C19–C24	120.7(5)	120.7
C4–C6–C7	128.4(5)	128.5	C20–C19–C24	117.1(5)	118.3
N11–C7–C6	113.3(4)	113.5	C19–C20–C21	121.7(5)	121
N11–C7–C8	101.5(4)	101.6	C20–C21–C22	119.2(5)	119.4
C6–C7–C8	114.4(5)	114.3	Cl25–C22–C21	119.6(4)	119.5
C7–C8–C9	102.5(4)	102.4	Cl25–C22–C23	120.0(5)	119.6
N10–C9–C8	113.7(5)	112.9	C21–C22–C23	120.5(6)	120.9
N10–C9–C19	122.4(5)	122.1	C22–C23–C24	120.3(6)	119.2
C8–C9–C19	123.6(5)	125	C19–C24–C23	121.3(5)	121.2
Correlation Coefficient (CC)					0.9954

Table 5. Torsion angles (°) of compound **5d**.

Atoms	XRD	DFT	Atoms	XRD	DFT
C6–S1–C2–C3	-0.5	-0.2	N11–C7–C8–C9	-12.8(5)	-6
C2–S1–C6–C4	0.5(4)	0.1	C7–C8–C9–C19	-176.0(5)	-177.9
C2–S1–C6–C7	-176.2(5)	-176.5	C7–C8–C9–N10	9.7(6)	3.5
C9–N10–N11–C7	-7.9(5)	-5.4	N10–C9–C19–C24	-177.7(5)	-180
C9–N10–N11–C12	-161.6(5)	-161.6	C8–C9–C19–C20	-170.8(5)	-178.6
N11–N10–C9–C8	-1.7(6)	0.9	C8–C9–C19–C24	8.5(8)	1.6
N11–N10–C9–C19	-176.1(5)	-177.7	N10–C9–C19–C20	3.1(8)	-0.2
C12–N11–C7–C8	165.2(4)	161.8	N11–C12–C13–C14	174.5(5)	179.5
N10–N11–C12–C13	160.8(5)	167.8	C17–C12–C13–C14	-1.5(8)	0.3
C7–N11–C12–C17	-173.7(5)	-166.1	N11–C12–C17–C16	-173.7(5)	-179.4
N10–N11–C7–C6	136.4(4)	130.4	C13–C12–C17–C16	2.4(8)	-0.1
N10–N11–C7–C8	13.2(5)	7.2	C12–C13–C14–Cl18	176.9(4)	179.8
N10–N11–C12–C17	-23.3(7)	-12.9	C12–C13–C14–C15	0.6(8)	-0.2
C12–N11–C7–C6	-71.6(6)	-74.9	Cl18–C14–C15–C16	-176.8(4)	-180
C7–N11–C12–C13	10.3(7)	14.6	C13–C14–C15–C16	-0.6(8)	-0.1
S1–C2–C3–C4	1.1(6)	0.3	C14–C15–C16–C17	1.5(8)	0.2
C2–C3–C4–C6	-0.8(7)	-0.2	C15–C16–C17–C12	-2.4(8)	-0.1
C2–C3–C4–C5	179.0(5)	178.8	C9–C19–C20–C21	178.6(6)	179.6
C5–C4–C6–S1	-179.7(4)	-178.9	C24–C19–C20–C21	-0.7(9)	0.2
C5–C4–C6–C7	-3.4(9)	-2.6	C9–C19–C24–C23	-179.3(5)	-179.7
C3–C4–C6–S1	0.1(6)	0.1	C20–C19–C24–C23	-0.1(8)	-0.1
C3–C4–C6–C7	176.4(5)	176.3	C19–C20–C21–C22	1.5(9)	0.2
C4–C6–C7–N11	145.2(5)	145.9	C20–C21–C22–Cl25	-179.7(5)	-180
C4–C6–C7–C8	-99.1(7)	-98.2	C20–C21–C22–C23	-1.6(10)	-0.1
S1–C6–C7–C8	77.0(5)	77.8	Cl25–C22–C23–C24	179.0(5)	180
S1–C6–C7–N11	-38.8(6)	-38.2	C21–C22–C23–C24	0.9(10)	0.1
C6–C7–C8–C9	-135.2(5)	-128.6	C22–C23–C24–C19	-0.1(9)	0.1
Correlation Coefficient (CC)					0.9995

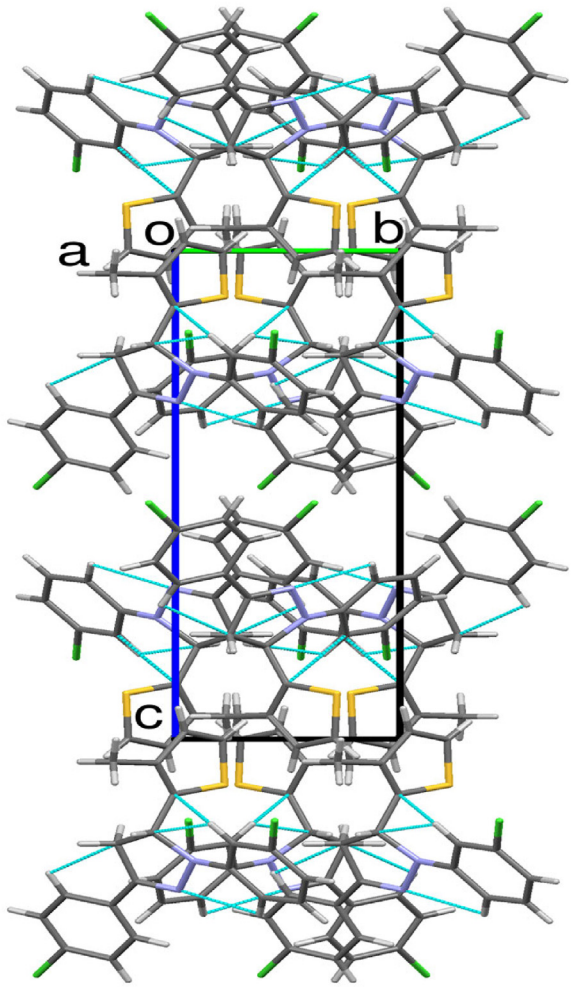

Figure 5. A perspective view of a supramolecular network by hydrogen bond interactions of the molecules **5d** along the *a*-axis.

7.345–7.384 (t, 2H, Ar–H), 7.853 (d, 2H, Ar–H); ^{13}C NMR ($CDCl_3$, δ ppm): 13.90 (1C, CH_3), 45.82 (1C, C-4), 54.45 (1C, OCH_3), 55.43 (1C, C-5), 111.55 (1C), 120.60 (2C), 120.80 (1C), 122.22 (2C), 129.06 (2C), 130.12 (2C), 131.33 (2C), 133.34 (1C), 139.46 (1C), 151.99 (1C), 155.40 (1C), 158.10 (1C, C-3). MS (*m/z*): 348.0 (M+, 100); Anal. Calcd. (found) for $C_{21}H_{20}N_2OS$ (%): C, 72.38 (72.31); H, 5.79 (5.75); N, 8.04 (8.01).

*2.2.6. 1-(3-Chlorophenyl)-3-(3-methoxyphenyl)-5-(3-methylthiophen-2-yl)-4,5-dihydro-1H-pyrazole, **5f***

Obtained from 1-(3-methoxyphenyl)-3-(3-methylthiophen-2-yl)prop-2-en-1-one, **3d** (1.27g, 5 mmol) and 3-chlorophenylhydrazine hydrochloride, **4b** (0.89g, 5 mmol); ^{1}H NMR ($CDCl_3$, δ ppm): 2.287 (s, 3H, CH_3), 3.161–3.217 (dd, 1H, *J* = *4.8, 17.*6Hz, C_4-H_a), 3.680–3.737 (dd, 1H, *J* = *5.2, 11.*2Hz, C_4-H_b), 3.827 (s, 3H, OCH_3), 5.744–5.786 (dd, 1H, *J* = *4.8, 11.*6Hz, C_5–H), 6.736 (s, 1H, Ar–H), 6.821–7.030 (m, 4H, Ar–H), 7.206–7.322 (m, 5H, Ar–H); ^{13}C NMR ($CDCl_3$, δ ppm): 13.91 (1C, CH_3), 42.71 (1C, C-4), 54.50 (1C, OCH_3), 55.36 (1C, C-5), 111.39 (1C), 116.07 (2C), 119.13 (2C), 122.46 (2C), 129.74 (2C), 130.20 (2C), 132.63 (1C), 133.49 (1C), 139.10 (1C), 151.68 (1C), 155.26 (1C), 159.76 (1C, C-3), 162.93 (1C). MS (*m/z*): 384.0 (M+2, 33), 382.0 (M+, 100); Anal. Calcd. (found) for $C_{21}H_{19}ClN_2OS$ (%): C, 65.87 (65.81); H, 5.00 (4.96); N, 7.32 (7.28).

*2.2.7. 5-(3-Methylthiophen-2-yl)-1-phenyl-3-(p-tolyl)-4,5-dihydro-1H-pyrazole, **5g***

Obtained from 3-(3-methylthiophen-2-yl)-1-(p-tolyl)prop-2-en-1-one, **3e** (1.42g, 10 mmol) and phenylhydrazine hydrochloride, **4a** (0.72g, 5 mmol); ^{1}H NMR ($CDCl_3$, δ ppm): 2.298 (s, 3H, CH_3), 2.378 (s, 3H, CH_3), 3.152–3.213 (dd, 1H, *J* = *7.6, 16.*8 Hz, C_4-H_a), 3.768–3.841 (dd, 1H, *J* = *12.0, 20.*8Hz, C_4-H_b), 5.389–5.438 (dd, 1H, *J* = *7.6, 12.*0Hz, C_5–H), 6.744–6.841 (d, 3H, Ar–H), 7.047–7.247 (m, 6H, Ar–H), 7.609–7.629 (d, 2H, Ar–H); ^{13}C NMR ($CDCl_3$, δ ppm): 14.43 (1C, CH_3), 42.06 (1C, C-4), 60.50 (1C, C-5), 110.72 (1C), 113.29 (1C), 119.05 (1C), 125.74 (1C), 125.90 (1C), 128.00 (1C), 129.18 (2C), 129.35 (1C), 129.82 (2C), 130.03 (1C), 132.42 (1C), 134.07 (1C), 134.97 (1C), 139.42 (1C), 145.24 (1C), 148.31 (1C, C-3). MS (*m/z*): 332.0 (M+, 100); Anal. Calcd. (found) for $C_{21}H_{20}N_2S$ (%): C, 75.87 (75.82); H, 6.06 (6.03); N, 8.43 (8.40).

*2.2.8. 3-(3,4-Dimethoxyphenyl)-5-(3-methylthiophen-2-yl)-1-phenyl-4,5-dihydro-1H-pyrazole, **5h***

Obtained from 1-(3,4-dimethoxyphenyl)-3-(3-methylthiophen-2-yl) prop-2-en-1-one, **3f** (1.44g, 5 mmol) and phenylhydrazine hydrochloride, **4a** (0.72g, 5 mmol); ^{1}H NMR ($CDCl_3$, δ ppm): 2.314 (s, 3H, CH_3), 3.142–3.204 (dd, 1H, *J* = *8.0, 17.*2Hz, C_4-H_a), 3.722–3.762 (dd, 1H, *J* = *4.4, 13.*2Hz, C_4-H_b), 3.864 (s, 3H, OCH_3), 5.425–5.475 (dd, 1H, *J* = *8.0, 12.*0Hz, C_5–H), 6.799–6.912 (m, 4H, Ar–H), 7.042–7.153 (m, 2H, Ar–H), 7.207–7.410 (d, 4H, Ar–H); ^{13}C NMR ($CDCl_3$, δ ppm): 13.95 (1C, CH_3), 42.94 (1C, C-4), 55.44 (1C, OCH_3), 55.47 (1C, OCH_3), 59.47 (1C, C-5), 110.64 (1C), 112.82 (1C), 113.83 (1C), 114.20 (1C), 124.32 (1C), 126.27 (1C), 127.44 (1C), 128.91 (1C), 129.57 (1C), 130.12 (1C), 130.32 (1C), 133.92 (1C), 135.66 (1C), 139.72 (1C), 145.27 (1C), 147.25 (1C), 159.72 (1C, C-3). MS (*m/z*): 378.1 (100); Anal. Calcd. (found) for $C_{22}H_{22}N_2O_2S$ (%): C, 69.81 (69.74); H, 5.86 (5.83); N, 7.40 (7.36).

*2.2.9. 1-(3-Chlorophenyl)-3-(3,4-dimethoxyphenyl)-5-(3-methylthiophen-2-yl)-4,5-dihydro-1H-pyrazole, **5i***

Obtained from 1-(3,4-dimethoxyphenyl)-3-(3-methylthiophen-2-yl) prop-2-en-1-one, **3f** (1.44g, 5 mmol) and 3-chlorophenylhydrazine hydrochloride, **4b** (0.89g, 5 mmol); ^{1}H NMR ($CDCl_3$, δ ppm): 2.304 (s, 3H, CH_3), 3.146–3.207 (dd, 1H, *J* = *7.6, 17.*2Hz, C_4-H_a), 3.767–3.839 (dd, 1H, *J* = *12.0, 16.*8Hz, C_4-H_b), 3.903 (s, 3H, OCH_3), 3.977 (s, 3H, OCH_3), 5.379–5.428 (dd, 1H, *J* = *7.6, 12.*0Hz, C_5–H), 6.75–6.851 (m, 4H, Ar–H), 7.039–7.089 (m, 3H, Ar–H), 7.21–7.251 (m, 1H, Ar–H), 7.481 (s, 1H, Ar–H); ^{13}C NMR ($CDCl_3$, δ ppm): 13.92 (1C, CH_3), 43.14 (1C, C-4), 55.93 (1C, OCH_3), 55.99 (1C, OCH_3), 59.10 (1C, C-5), 108.29 (1C), 110.62 (1C), 111.33 (1C), 113.85 (1C), 119.26 (1C), 119.39 (1C), 123.61 (1C), 125.20 (1C), 129.81 (1C), 130.34 (1C), 132.79 (1C), 134.66 (1C), 139.10 (1C), 146.32 (1C), 148.29 (1C), 149.18 (1C), 150.26 (1C, C-3). MS (*m/z*):

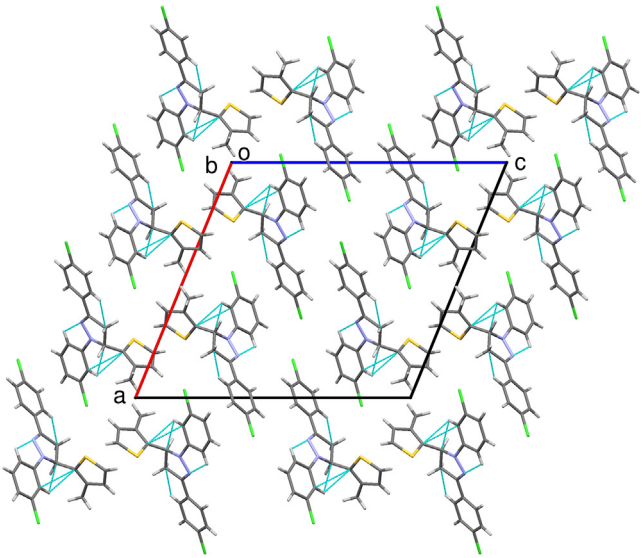

Figure 6. A perspective view of a supramolecular network by hydrogen bond interactions of the molecules **5d** along the *b*-axis.

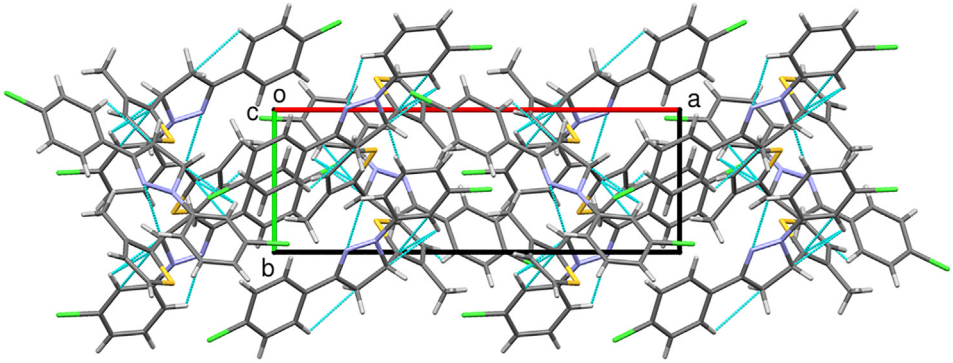

Figure 7. A perspective view of a supramolecular network by hydrogen bond interactions of the molecules **5d** along the *c*-axis.

414.2 (M+, 33), 412.22 (M+, 100); Anal. Calcd. (found) for $C_{22}H_{21}ClN_2O_2S$ (%): C, 63.99 (63.92); H, 5.13 (5.10); N, 6.78 (6.72).

2.3. X-ray diffraction studies

The brown colored prismatic defect free single crystal of approximate dimension 0.27 × 0.24 × 0.21 mm^3 was chosen for X-ray diffraction studies. The X-ray intensity data of the molecule **5d** were collected using Rigaku XtaLAB Mini diffractometer with X-ray generator operating at 50 kV, 12 mA and MoK_α radiation. Data were collected with χ fixed at 54°, for different settings of ϕ (0° and 360°), the scan width of 0.5° with exposure time of 3 s and the sample to detector distance of 50 mm. The complete data sets were processed by *CRYSTAL CLEAR* [24]. The crystal structures were solved by *SHELXS* and *SHELXL* programs [25, 26]. The geometrical calculations were performed with *PLATON* [27]. The molecular and packing diagrams were generated using *MERCURY* [28].

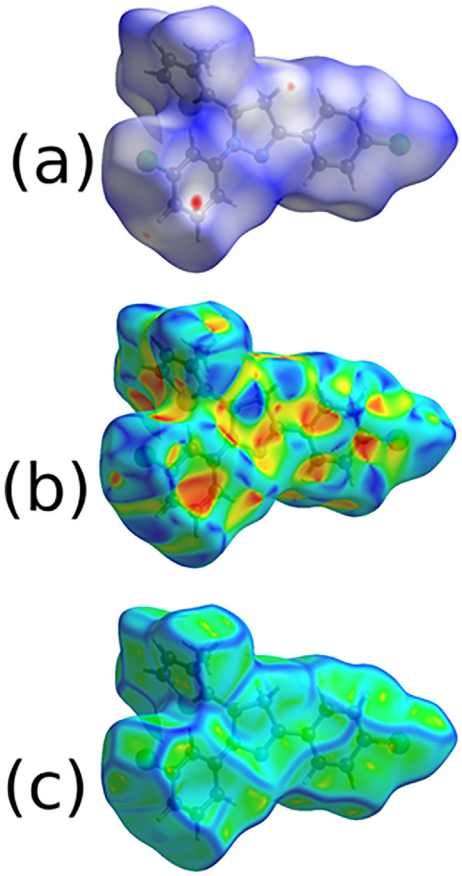

Figure 8. (a) d_{norm}; (b) shape index and (c) curvedness mapped on Hirshfeld surface of the molecule **5d**.

2.4. Biological activity

2.4.1. DPPH radical scavenging activity

The activity of compounds **5(a–i)** was performed by a Blois method [29], with different concentrations (2.5, 5.0, 7.5 and 10.0 μM) in methanol. The absorbance was read against blank at 517 nm.

2.4.2. Hydroxyl radical scavenging activity

The experiments were performed according to reported procedure [30]. A solution of phosphate buffer (0.1 mL); 2-deoxyribose (0.2 mL), compounds, **5(a–i)** (2.5, 5.0, 7.5 and 10.0 μM), Hydrogen peroxide (0.1 mL, 10 mM), ascorbic acid (0.1 mL, 1 mM), EDTA (0.1 mL), and Ferric chloride (0.01 mL, 100 mM) was incubated at 37 °C for 60 min. After this, a cold 2.8% trichloroacetic acid (1mL) followed by 1% thiobarbituric acid (1mL, 1g/100mL of 0.05 N NaOH) were added, and kept for 15 min in boiling water. The absorbance measured at 535 nm.

2.5. Molecular docking studies

The co-ordinates of Catalase (CAT) (PDB id: 2CAG) and CuZn superoxide dismutase (CuZnSOD) (PDB id: 1CB4) were collected from the Brookhaven Protein Data Bank [31]. The minimal energy of ligands was computed by OPLS 2005. Proteins prepared by retrieving into workspace, and their structure were corrected by prime software module. Water molecules from CAT and CuZnSOD were removed beyond 5 Å from the hetero atoms. The interaction between the receptor, and water molecules were optimized during protein pepwizard [32]. OPLS 2005 force field applied to the protein to restrain minimization and RMSD of 0.30 Å was set to converge heavy atoms before start of docking. Each ligand was docked into the receptor grid of radii 20 Å, and the docking calculation was performed. ADME/Tox properties were calculated with ADME/Tox prediction program [33].

3. Results and discussion

The current investigation presents the synthesis of new pyrazole derivatives, structural characterisation by spectral and crystallographic studies; which follows the assessment of new compounds for their antioxidant activities. Further, to substantiate with the experimental results, the molecular docking and ADMET analysis was performed to substantiate the experimental results. The flowchart showing the methodology is presented on Figure 1. A library of trisubstituted pyrazoles prepared were presented in Figure 2.

3.1. Chemistry

A two-step synthesis of different tri-substituted pyrazole products was performed. In the first step, the required chalcones, **3(a-f)** were prepared from thiophene-2-aldehyde **1**, with various substituted acetophenone, **2(a-f)** in line with our earlier report [34]. In the second step, the

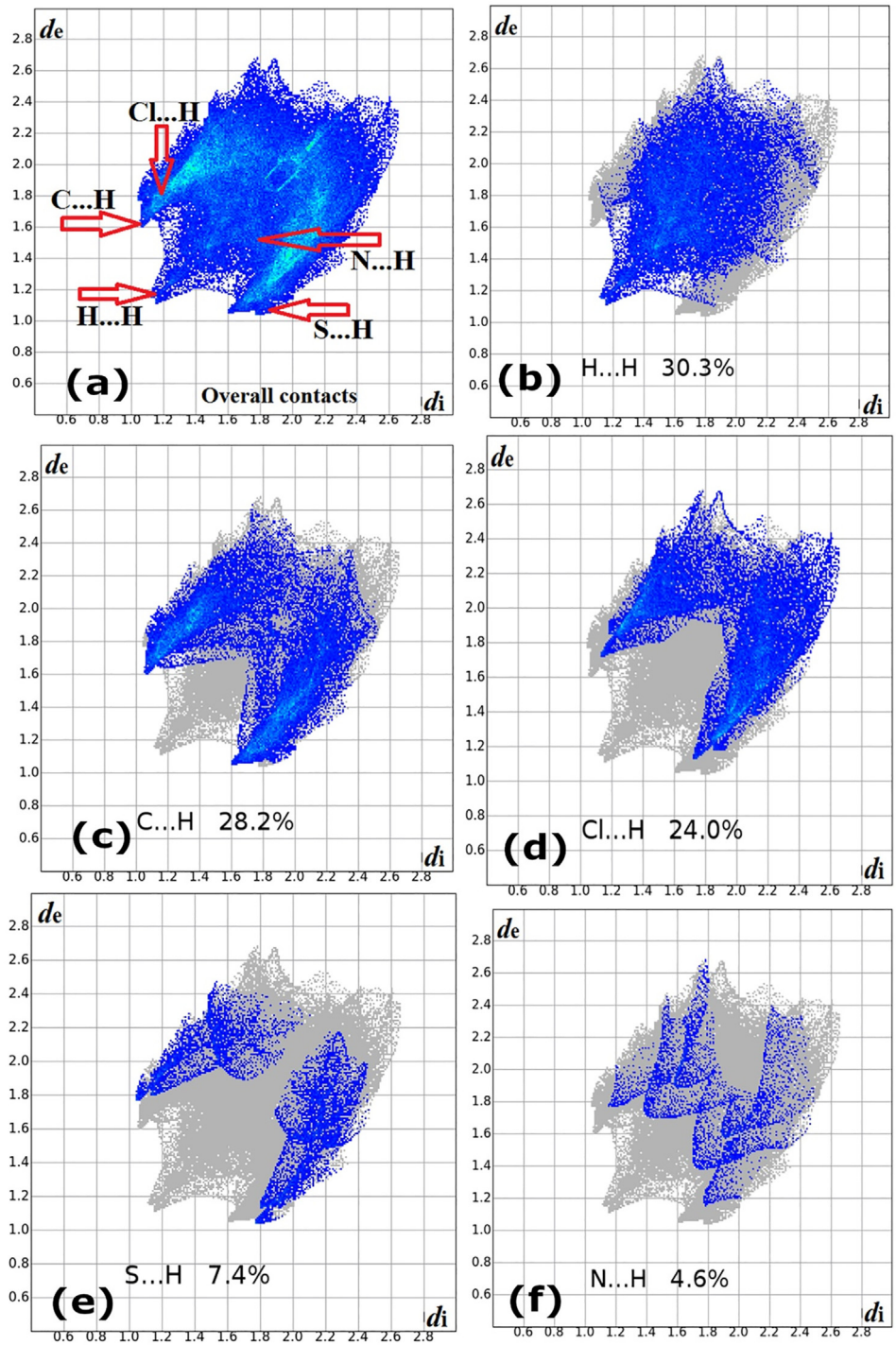

Figure 9. 2D fingerprint plot of molecule **5d** displaying the intermolecular (a) Overall contact, (b) H···H, (c) C···H, (d) Cl···H, (e) S···H, and (f) N···H interactions.

chalcones **3(a-f)** were subjected to Amberlyst-15 (10%, w/w) catalyzed (3 + 2) annulation reaction with phenylhydrazine hydrochloride **4(a-b)** in acetonitrile as solvent. The reaction was performed under swirling conditions. The reaction produced thienyl-pyrazoles, **5(a-i)** in good yields. In an alternative method, the compounds **5(a-i)** were also obtained by reflux conditions in 30% acetic acid medium without an added catalyst. In this research, cyclocondensation of the chalcones, and phenylhydrazine hydrochlorides produced desired trisubstituted pyrazole derivatives (Figure 3).

Amberlyst-15, (divinylbenzene-styrenesulfonic acid) is a versatile catalyst for the reactions under non-aqueous conditions, it promotes the reaction through its $-SO_3H$ proton, in esterification, Prins cyclization, and crossed-aldol condensation etc., [35]. We found that Amberlyst-15 catalyzed synthesis of pyrazole derivatives **5(a-i)** occurs in less time with minimum heat energy compared, and an improved product yields (>4–9%) comparable to the conventional reflux conditions method in acetic acid (Table 1). The recovered catalyst can be re-used efficiently.

3.2. Spectroscopic studies

In the ^{1}H NMR spectra, compounds **5(a-i)** show that $-CH_2-$ group of the pyrazole ring diastereotopic; and failed to show the signals of C=C

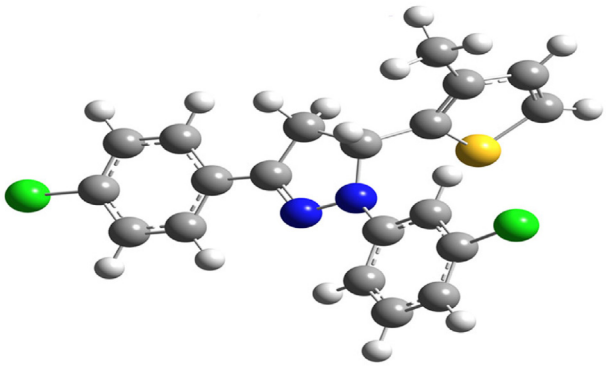

Figure 10. The optimized structure of molecule **5d**.

Table 6. FMO energies and chemical reactive descriptors of molecule **5d**.

Parameters	Value [B3LYP/6–311++G(d,p)] (eV)
E_{HOMO}	-5.3005
E_{LUMO}	-1.4749
E_{gap}	3.8256
Ionization potential (I)	5.3005
Electron affinity (A)	1.4749
Electronegativity (χ)	3.3877
Chemical hardness (η)	1.9128
Global softness (σ)	0.5228
Electrophilicity (ω)	2.9999
Chemical potential (μ)	-3.3877
Dipole moment (D)	2.9618

Where, $\chi = (I + A)/2$, $\eta = (I\text{-}A)/2$, $\sigma = 1/\eta$ and $\omega = \mu^2/2\eta$.

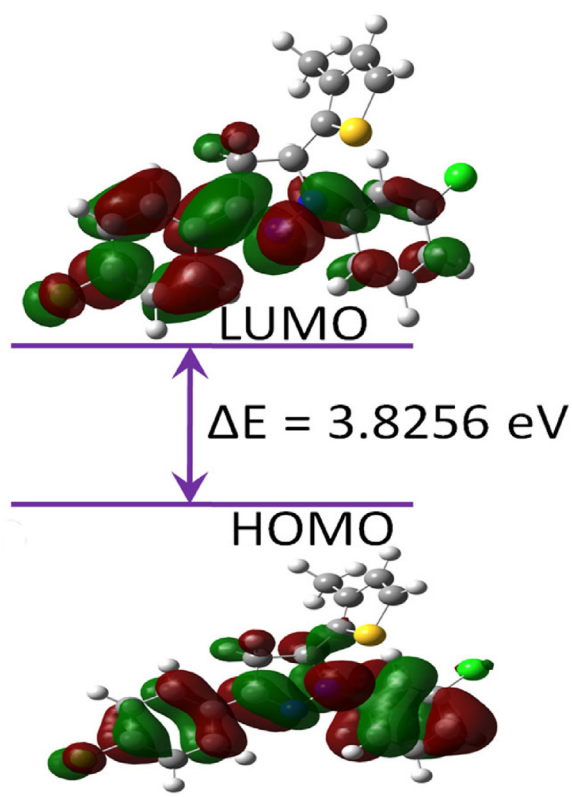

Figure 11. FM orbitals (HOMO-LUMO) with energy gap of a moleucle **5d**.

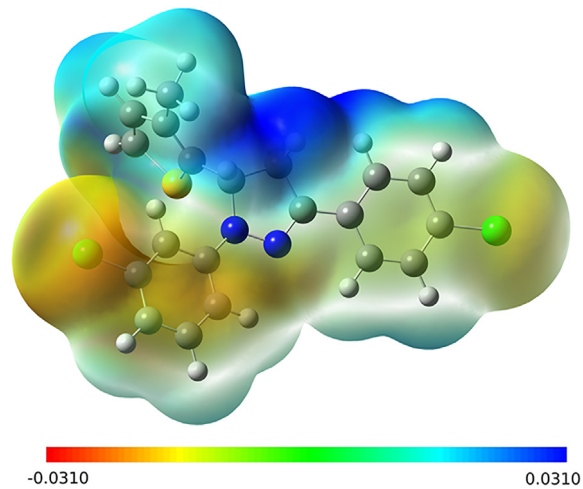

Figure 12. Molecular electrostatic potential map of a molecule **5d**.

protons of **3(a-f)**, confirming the (3 + 2) annulation. In ^{1}H NMR spectrum, compound **5i** show a doublet of doublets for C_4-H_a at δ 3.146–3.207 (*J = 7.6, 17.*2 Hz) ppm; C_4-H_b at δ 3.767–3.839 (*J= J = 12.0, 16.*8 Hz) ppm, and C_5–H at δ 5.379–5.428 (*J= J = 7.6, 12.*0 Hz) ppm. It shows singlets for CH_3 at δ 2.304 ppm, for two OCH_3 at δ 3.903, δ 3.977 ppm, and multiplet at δ 6.750–6.851 ppm, δ 7.039–7.089 ppm, δ 7.215–7.481 ppm for aromatic protons. In ^{13}C NMR spectrum, it shows signals for C-4, C-5 and C-3 carbons of pyrazoline ring at δ 43.14, 59.10 and 150.26 ppm, respectively. It also shows signals for CH_3 at δ 13.92 ppm, for two OCH_3 carbons at δ 55.93 and δ 55.99 ppm. In mass spectrum, it shows peaks at m/z 415.2 (M+2) (34%), 413.2 (M+). It shows comparable CHN analysis data with the theoretical values. Analytical and spectral data (^{1}H & ^{13}C NMR, MS) for all compounds **5(a-i)** were in full agreement with the proposed structures, and also structurally related pyrazoles [35]. Furthermore, the structure of one compound **5d**, of the series was provided by crystallographic studies.

3.3. Single crystal X-ray diffraction studies

The crystallographic data and structure refinement data of 5d are depicted in Table 2. The *ORTEP* of the molecule with the thermal ellipsoids drawn with 50% probability is shown in Figure 4. The bond length, bond angles and torsion angles are summarized in Tables 3, 4 and 5. The compound has four aromatic rings, viz; a pyrazole, thiophene, and two chlorophenyl rings. Thiophene ring is planar (r.m.s. deviation is 0.007(5)

Table 7. DPPH and hydroxyl radical scavenging activity of the compounds, **5(a-i)**.

Compounds	DPPH radical assay	Hydroxyl radical assay
	IC_{50} (μM)[a]	IC_{50} (μM)[b]
5a	0.807 ± 0.01	3.534 ± 0.01
5b	0.488 ± 0.02	1.439 ± 0.01
5c	0.529 ± 0.02	1.813 ± 0.01
5d	0.673 ± 0.01	2.641 ± 0.02
5e	0.616 ± 0.03	1.965 ± 0.04
5f	0.694 ± 0.04	2.649 ± 0.02
5g	0.245 ± 0.01	0.905 ± 0.01
5h	0.284 ± 0.02	0.892 ± 0.01
5i	0.491 ± 0.01	1.913 ± 0.04
AA*	0.483 ± 0.01	–
BHA**	–	1.739 ± 0.01

*Ascorbic acid; **Butylated hydroxyanisole were used as controls; [a,b]values represent mean ± SEM (n = 3).

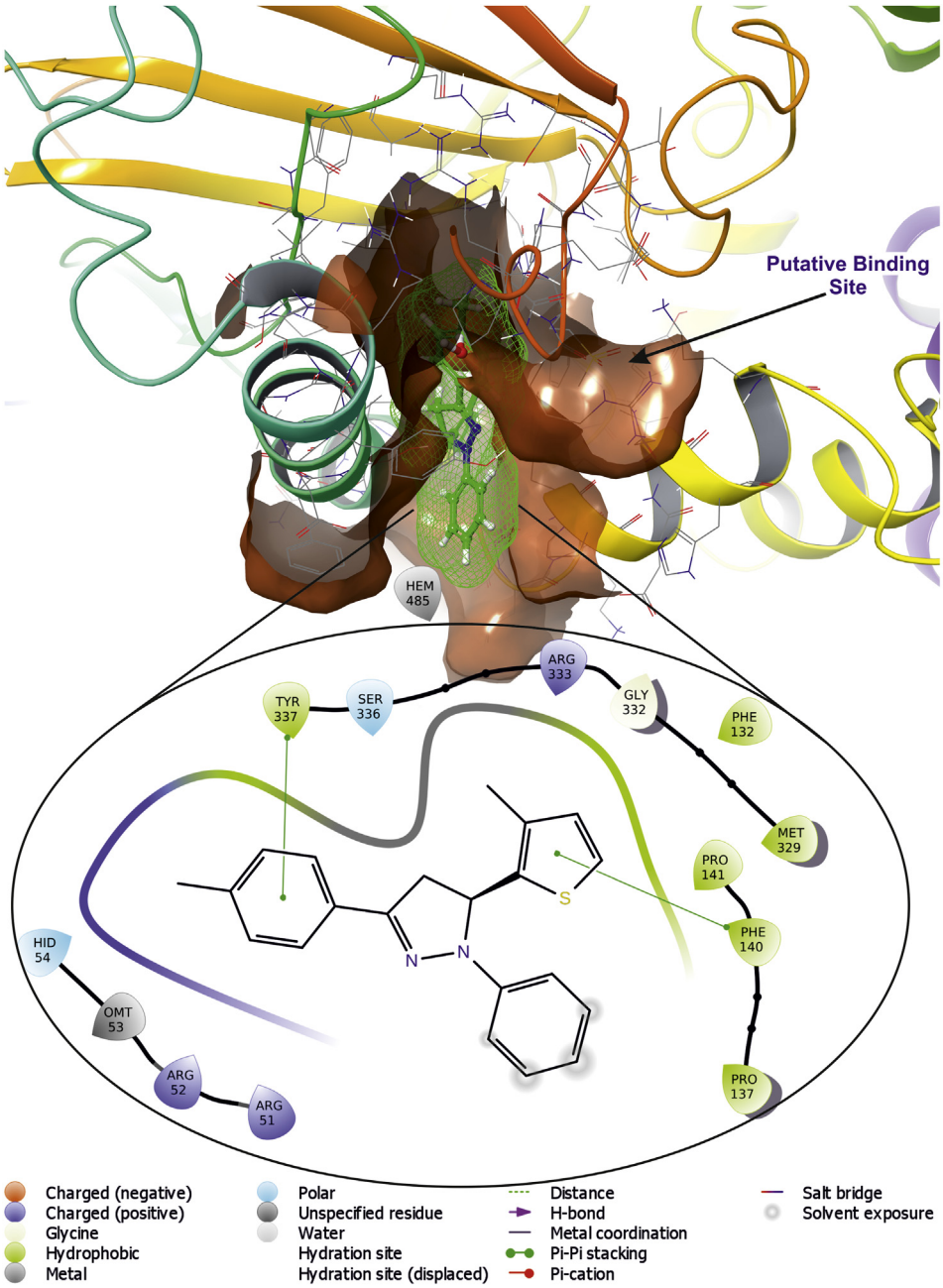

Figure 13. The putative binding pose of compound **5g** with Catalase (PDB ID: 2CAG); the ligand **5g** is represented as green wire mesh deeply embedded into active site.

Å) with maximum deviation (0.006(6) Å) observed for atoms C2 and C3. Pyrazole ring is little non-planar (r.m.s. deviation is 0.096(5) Å) with maximum deviation of 0.082(6) Å for atom C7. Among two chlorophenyl rings, 3-dichlorophenyl ring is planar (r.m.s. deviation is 0.010(6) Å) with maximum deviation (0.012(6) Å) observed for atom C17. Similarly, 4-chlorophenyl ring is also planar (r.m.s. deviation is 0.007(6) Å) with a deviation of 0.008(7) Å for atom C21. The methylthiophene ring is fixed at C7, 3-dichlorophenyl ring fixed at N11, 4-chlorophenyl ring is fixed at C9 and benzodioxole ring is fixed at C11 atom of the pyrazole ring. The chlorine atoms substituted to the corresponding phenyl rings are in the same plane of the rings.

A dihedral angle of 76.3(3)^{o} between the pyrazole and thiophene ring indicates that they lie in different planes. Similarly, the angle between thiophene to 3-chlorophenyl and 4-chlorophenyl rings are 86.5(3)^{o} and 74.1(3)^{o} respectively. The dihedral angle of 13.5(3)^{o,} and 4.0(3)^{o} between pyrazole ring with 3-chlorophenyl and 4-chlorophenyl rings indicates that these coplanar. The analyzed Cremer and Pople puckering parameters (Q = 0.136(6) Å and ϕ = 78(2)^{o}) were in agreement with the structurally identical molecules [36, 37]. The ring has envelope conformation on C7 atom with rotation parameters value of P = 238.9(14)^{o} and τ = 14.1(3)^{o}. The C–H·····N hydrogen bond and C–H····π and π····π interactions stabilized the structure: The C17–H17· · · N10 intramolecular hydrogen bond interactions forms five membered pseudo ring (N10/N11/C12/C17/H17). Also the other molecular interactions such as, C–H····π interaction: C2–H2····Cg1 with a C−Cg distance of 3.512(6) Å, H····Cg distance of 2.77 Å and C–H····Cg angle of 137°; C7–H7····Cg3 with a C−Cg distance of 3.735(6) Å, H· · · Cg distance of 2.93 Å and C–H····Cg angle of 140°; C15–H15····Cg4 with a C−Cg distance of 3.567(7) Å, H· · · Cg distance of 2.74 Å and C–H····Cg angle of 148°. π····π interaction: Cg2····Cg3 with a Cg − Cg distance of 3.956(4) Å, α =

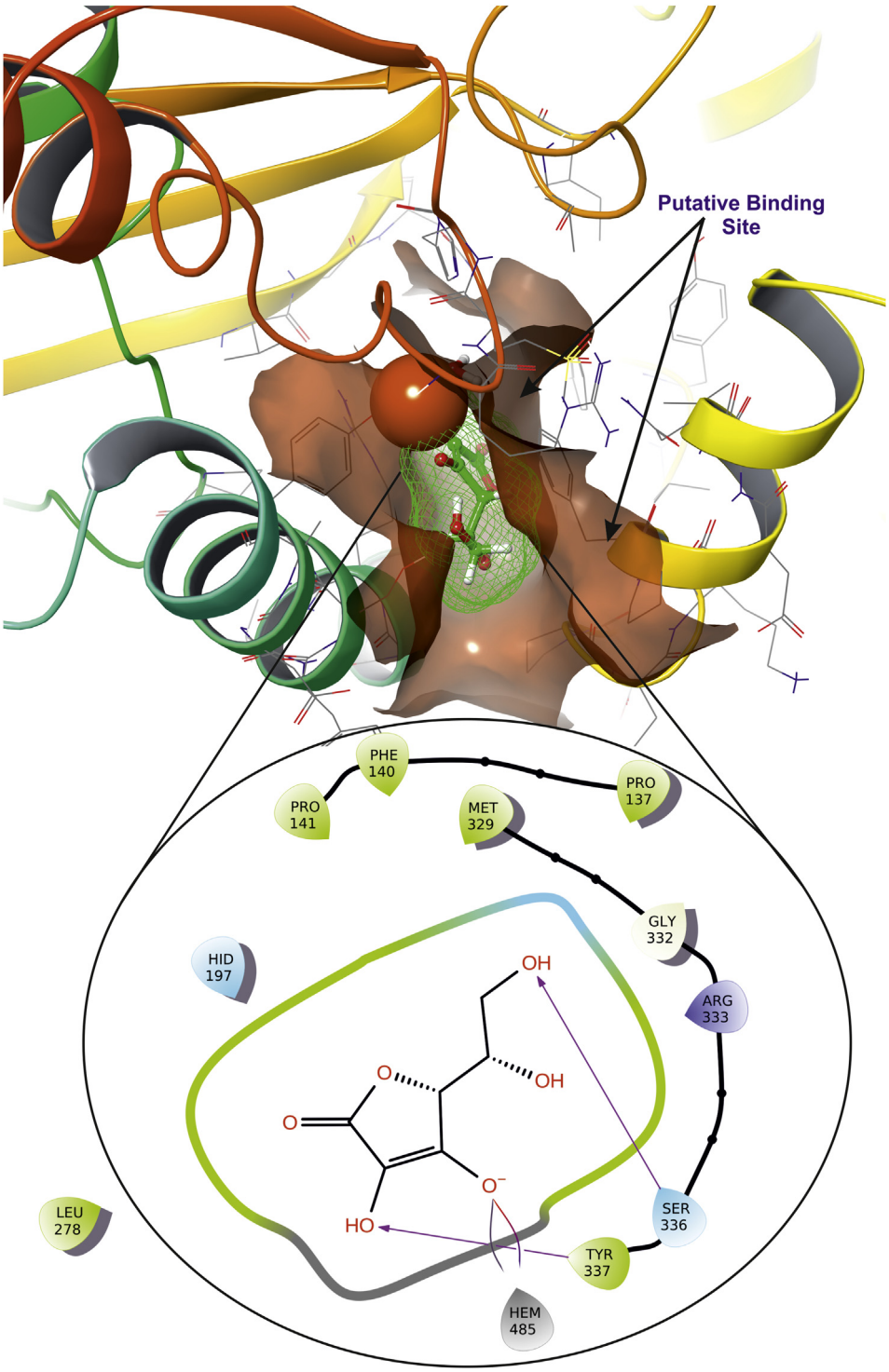

Figure 14. The putative binding pose of standard ascorbic acid with Catalase (PDB ID: 2CAG); Ascorbic acid is represented as green wire mesh deeply embedded into active site.

13.5(3)°, β = 22.7°, γ = 28.5° and a perpendicular distance of Cg2 on ring Cg3 = 3.649(2) Å. The packing of the molecules viewed across *a, b* and *c*-axis showing the layered stacking are depicted in Figures 5, 6, and 7, respectively.

3.4. Hirshfeld surface analysis

With CrystalExplorer 17.5, the 3D d norm was mapped on Hirshfeld surface (HS) with colour scale in between -0.583 au (blue) to 1.359 au (red). The calculated volume of the Hirshfeld surface is 451.41 Å^3 with an area of 402.38 Å^2. The 2D fingerprint plots were generated at 0.6–2.8 Å, with d_i and d_e distance scales.

In the d_{norm} (Figure 8a), colour codes indicate the different molecular interactions; red with negative $d_{norm,}$ white with zero $d_{norm,}$ and blue with positive d_{norm} indicates the short contacts, intermolecular distances equal to van der Waals radii, and longer contacts [38, 39], respectively. Figure 9 shows the expanded 2D fingerprint plots [40] with the d_e and d_i distance scales. The finger print plot reveals the contribution of overall

Table 8. Docking scores of the newly synthesized compound **5(a-i)** against Catalase and CuZn superoxide dismutase. Docking scores and Glide energies (kcal/mol) as obtained through Glide docking.

Protein	Catalase (PDB id: 2CAG)				CuZn superoxide dismutase (PDB id: 1CB4)			
Ligand	Docking Score (kcal/mol)	G_{Energy} (kcal/mol)	G_{Emodel} (kcal/mol)	XP Hbond (kcal/mol)	Docking Score (kcal/mol)	G_{Energy} (kcal/mol)	G_{Emodel} (kcal/mol)	XP Hbond (kcal/mol)
5a	-3.26	-31.73	-42.14	-0.27	1.93	-30.29	-39.26	0.00
5b	-3.74	-33.95	-42.02	-0.70	-1.20	-33.28	-42.85	-0.05
5c	0.07	-39.67	-44.00	0.00	-1.08	-32.85	-41.16	-0.21
5d	-3.90	-36.88	-48.85	-0.70	1.85	-32.80	-41.69	0.00
5e	-2.00	-30.77	-45.65	-0.13	0.16	-32.89	-39.33	0.00
5f	-2.31	-32.28	-46.86	-0.48	1.88	-34.93	-45.06	-0.08
5g	-5.41	-39.09	-60.37	-0.57	-1.23	-33.78	-43.78	-0.20
5h	-4.40	-41.81	-49.69	-0.01	1.56	-33.04	-44.76	-0.35
5i	-4.06	-47.53	-61.02	-0.02	1.85	-34.92	-48.88	-0.38
Ascorbic acid	**-9.25**	**-23.53**	**-37.25**	**-2.53**	**-4.24**	**-25.72**	**-26.66**	**-2.11**

contacts (Figure 9a) including each individual intermolecular contact to the total molecular HS. The contributions of various interactions; H–H (30.3%) [Figure 9b], C–H (28.2%) [Figure 9c], Cl–H (24.0%) [Figure 9d], S–H (7.4%) [Figure 9e], N–H (4.6%) [Figure 9f], C–Cl (1.9%), S–Cl (1.0%), Cl–Cl (0.9%), C–S (0.6%) and C–N (0.1%) were quantified through 2D fingerprint plots. The contribution of H···H contacts will be of 30.3% to the total Hirshfeld surface. The shape index, curvedness of HS were generated (Figure 8b and c) to analyze the π-stacking interactions [41, 42, 43].

3.5. Density functional theory (DFT) calculations

The electronic and chemical active regions of a compounds were identified with the quantum chemical calculations, FMO energies, and MEP surface analysis. The structural coordinates are optimized (Figure 10) in gas phase using DFT method with B3LYP hybrid functional and 6–311++G(d,p) basis set. The calculated structural parameters were compared with experimental results. The optimized structure substantiates the experimental findings with the correlation coefficient values; bond lengths (**0.9929**), bond angles (**0.9954**) and torsion angles (**0.9995**) (Tables 3, 4 and 5). Further, the FMO energies (E_{HOMO}, E_{LUMO} and E_g) and chemical reactive descriptors [44, 45, 46, 47] were calculated (Table 6).

The polarizability and chemical reactivity of a compound was assessed on the band gap energy. The FMO HOMO-LUMO energies with the calculated energy gap of $E_{gap} = 3.8256$ eV (Figure 11). The red and green colors on the molecular surface indicates the positive and negative phases of the wave functions. The MEP map drawn in the range of -3.100e^{-2} au (red) to +3.100 e^{-2} au (blue) (Figure 12). The positive (blue), and negative (green) regions of MEP represent an electrophilic and nucleophilic reactivity. The red regions are related to the electrophilic attack. The red and light blue colors are spread over chlorine and nitrogen, hydrogens [48], respectively.

3.6. Radical scavenging activity

The radicals are highly reactive and least stable species, formed during various metabolic processes that cause cellular damages in living cells, such as capable to break DNA and cause strand breakage [49]. In recent times, antioxidants display radical scavenging activity acts as anticancer, anti-inflammatory and antiaging agents [50]. Therefore, the antioxidant ability of new compounds **5(a-i)** was assessed by DPPH and Hydroxyl radical assay using ascorbic acid (AA) and Butylated hydroxyanisole (BHA), as control treatment. The experiments were performed in triplicates with varied concentrations. The IC50 values were computed by using graphpad Prism using equation Y=Bottom + (Top-Bottom)/(1 + 10((LogIC$_{50}$-X)*HillSlope)) from the observed percentage inhibition of the compounds **5(a-i)** (Table 7).

The preliminary assessment results indicated that each compound of series **5(a-i)** exhibit modest to good radical scavenging activities as compared with respective standards AA and BHA. Of the nine tested pyrazoles, five shown moderate to potent abilities in both the assays, indicating their reducing abilities.

The plausible mechanism involves the transfer of acidic H-atom by a compound to DPPH to form DPPH-H. The most active compounds were **5g**, and **5h** ($IC_{50} = 0.245 \pm 0.01$, and 0.284 ± 0.02 μM, respectively). These have potent RSA than ascorbic acid ($IC_{50} = 0.483 \pm 0.01$μM), indicating that, the electron donating methyl and methoxy substituents in 3-substituted aromatic ring increases the antioxidant activity of pyrazoles. The two molecules **5b** ($IC_{50} = 0.488 \pm 0.02$μM) and **5i** ($IC_{50} = 0.491 \pm 0.01$μM) shows good RSA, but lower than ascorbic acid activity. The rest of the compounds **5c** ($IC_{50} = 0.488 \pm 0.02$μM), **5e** ($IC_{50} = 0.488 \pm 0.02$μM), **5d** ($IC_{50} = 0.488 \pm 0.02$μM), **5f** ($IC_{50} = 0.488 \pm 0.02$μM), and **5a** ($IC_{50} = 0.488 \pm 0.02$μM), displayed moderate activities. Interestingly, all of these compounds showed the better antioxidant properties than the structurally related compounds, 5-(3,4-dichlorophenyl)-3′-naphthalen-2-yl-1′-phenyl-3,4-dihydro-1′H-[3,4′]bi pyrazoles reported, which showed DPPH radical scavenging activities in the range of $IC_{50} = 9.66 \pm 0.34$ to 12.02 ± 0.63μM [51].

In the Hydroxyl radical scavenging assay; the most active molecules were **5g** ($IC_{50} = 0.905 \pm 0.01$μM), and **5h** ($IC_{50} = 0.892 \pm 0.01$μM). They exhibited potent RSA than BHA ($IC_{50} = 1.739 \pm 0.01$μM). The compounds **5b** ($IC_{50} = 1.439 \pm 0.01$μM), and **5i** ($IC_{50} = 1.913 \pm 0.04$μM) shows good RSA, but lower than BHA. The rest of the compounds **5c** ($IC_{50} = 1.813 \pm 0.01$μM), **5e** ($IC_{50} = 1.965 \pm 0.04$μM), **5d** ($IC_{50} = 2.641 \pm 0.02$μM), **5f** ($IC_{50} = 2.649 \pm 0.02$μM), and **5a** ($IC_{50} = 3.534 \pm 0.01$μM), displayed moderate activities. However, all new compounds show better activities compared with the reported similar pyrazoles; like 1,3-diaryl-4-(aryl-propenonyl)-pyrazoles (IC_{50} = 13.5–13.5μM) [52], 3-(2-bromophenyl)-4-(4,5-diphenyl-1*H*-imidazole-2yl)-1-(p-tolyl)-1*H*-pyrazole (IC_{50} = 10.2μM) [53], N,N-bis((3,5-dimethyl-1*H*-pyrazol-1-yl)methyl)thiazol-2-amine (IC_{50} = 14.76μM) [54], suggesting that the new compounds of the present work could act as potent antioxidants. The presence of substituents on the two phenyl rings at 1,3 positions of pyrazole nucleus influences the RSA. The molecule **5a** of the series, with two unsubstituted benzene rings at 1 and 3 positions of pyrazole exhibited least activity in both assays. It was observed that the presence of the electron donating 4-methyl, 4-methoxy, and 3,4-dimethoxy groups on C-3 substituted aromatic ring enhanced the DPPH and OH radical scavenging activities.

3.7. Molecular docking and ADME/Tox predictions

Molecular docking studies for newly synthesized compounds suggest that the ligand **5h** and **5g** comparatively possess better antioxidant activity among **5(a-i),** as compared with the standard antioxidant molecule

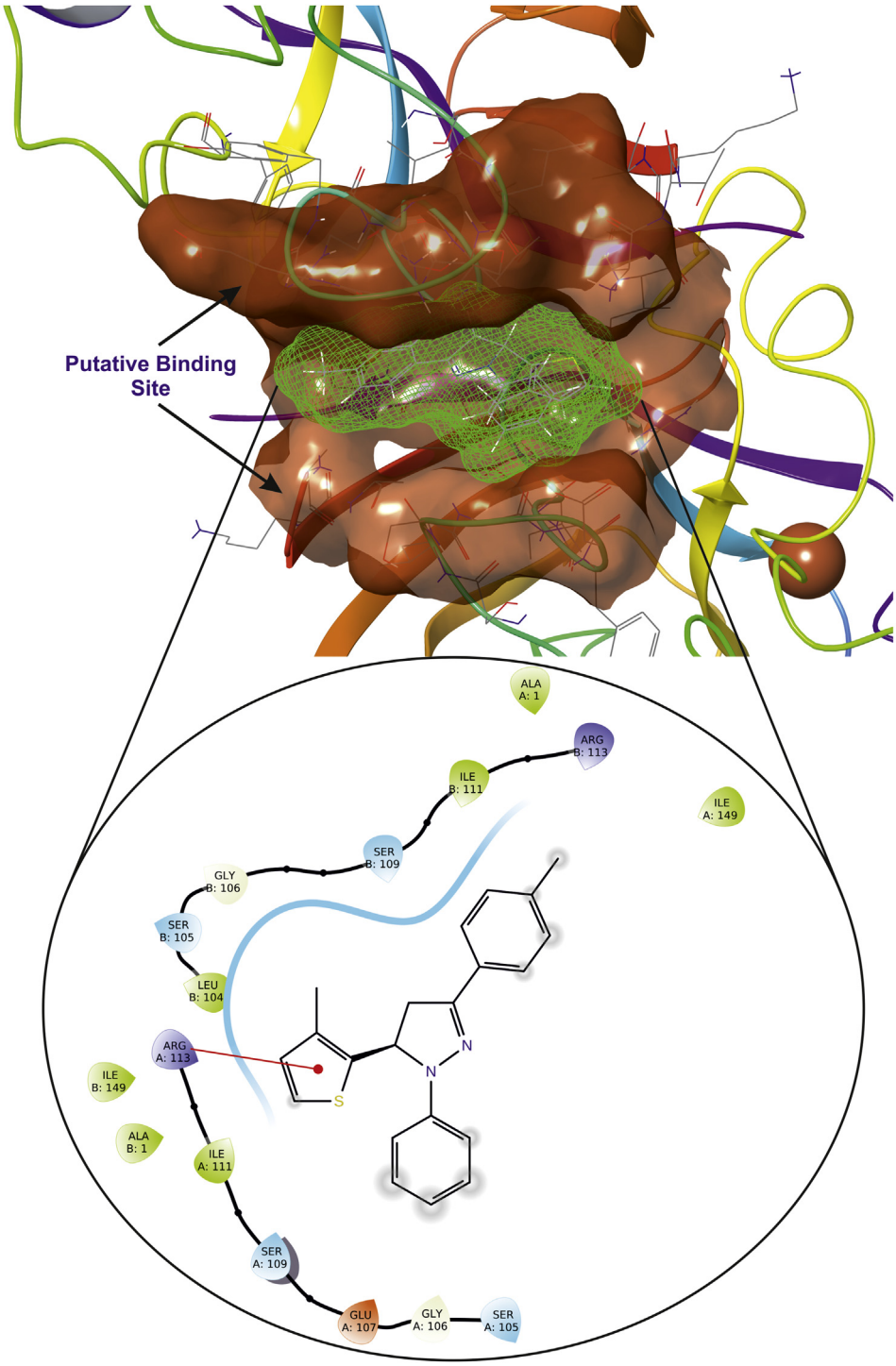

Figure 15. Putative binding pose of compound **5g** with CuZn superoxide dismutase (PDB ID: 1CB4); the ligand is represented as green wire mesh deeply embedded into active site.

such as ascorbic acid. Antioxidants play an important role in various patho-physiological disease conditions such as, cancer, chronic inflammation, diabetics, arthritis, neuro-degenerative disorder. Hence decrease in free radicals in these diseases' conditions, enhance the patho-physiological condition towards the normal [31]. The ligand **5g** forms π-π stacking with Catalase *via* Try337 and Phe140 (Figure 13) which are closely resided at active site, whereas ascorbic acid forms salt bridge with Arg333 and with Protoporphyrin IX containing Fe (Figure 14). Three-dimensional view of **5g** and ascorbic acid suggest that it is deeply embedded into active site surrounded with active site amino acids which is very important in aiding catalysis with dock score of -5.41 and -9.25 (kcal/mol) (Table 8).

Superoxide dismutase (SOD) is another very important enzyme which acts as antioxidant defense against oxidative stress in the body. The ligand **5g** form π-cation with Arg113 (Figure 15); while ascorbic acid form hydrogen bond with Ile111 and Gly106. The compound binds at Cu–Zn domain of SOD led to increase in an antioxidant activity and decrease in oxidative stress [52]. ADME/Tox properties depict that the ligands possess druggable properties, with 95% of available drugs which are in market. The results molecular docking (Table 8) and ADME

Table 9. *In silico* ADME/Tox screening of the new compounds **5(a-i)**.

Ligand	a*	b*	c*	d*	e*	f*	g*	h*	i*	j*	k*	l*	m*	n*	o*	p*
5a	40.35	11.48	14.01	5.31	6.28	-7.18	-6.56	-6.35	8246.1	0.56	7264.66	-0.07	1.41	1.00	100.0	1.00
5b	40.60	11.06	14.38	5.10	6.51	-7.54	-6.94	-6.23	8186.7	0.67	10000.00	-0.21	1.45	1.00	100.0	1.00
5c	44.58	12.62	16.03	5.35	7.24	-9.30	-7.67	-6.88	4473.6	0.54	10000.00	-0.79	1.76	1.00	100.0	1.00
5d	42.97	12.64	15.52	4.83	7.28	-8.66	-8.02	-6.18	8254.0	0.90	10000.00	-0.40	1.66	1.00	100.0	1.00
5e	42.20	11.81	14.91	5.55	6.34	-7.33	-6.85	-6.29	8288.3	0.50	7327.00	-0.16	1.38	1.00	100.0	1.00
5f	43.64	12.44	15.82	5.34	6.87	-8.12	-7.58	-6.25	8340.7	0.68	10000.00	-0.31	1.52	1.00	100.0	1.00
5g	42.41	11.70	14.62	5.01	6.65	-7.77	-6.86	-6.25	8570.2	0.58	7661.63	-0.22	1.60	1.00	100.0	1.00
5h	44.23	12.19	15.86	5.81	6.43	-7.53	-7.14	-6.25	8335.3	0.44	7336.01	-0.24	1.37	1.00	100.0	1.00
5i	45.50	12.76	16.60	5.56	6.92	-8.24	-7.87	-6.13	8306.8	0.61	10000.00	-0.41	1.50	1.00	100.0	1.00
Ascorbic acid	11.83	6.17	14.89	14.6	-1.85	-0.64	-0.76	-2.83	36.24	-1.81	13.71	-5.64	-0.95	2.00	44.01	0.00

Note: a*-QPpolrz; b*-QPlogPC16; c*-QPlogPoct; d*-QPlogPw; e*-QPlogPo/w; f*-QPlogS; g*-CIQPlogS; h*-QPlogHERG; i*-QPPCaco; j*-QPlogBB; k*-QPPMDCK; l*-QPlogKp; m*-QPlogKhsa; n*-Human Oral Absorption; o*-Percent Human Oral Absorption; p*-Rule of Five.

studies/Tox (Table 9) prove that, ligands **5h** and **5g** are potent with druggable properties without violation of the Lipinski's rule.

4. Conclusion

In summary, a novel thiophene-pyrazole pharmacophores **5(a-i)** were synthesized using a re-useable Amberlyst-15 catalyst, and assessed for their *in vitro* DPPH and Hydroxyl radical scavenging abilities. The fine structure of the compound **5d** is confirmed by crystallographic studies. The analysis revealed the presence of C–H···N type H-bond and stabilized by C–H...π and π—π interactions. The chemically reactive regions were identified by HSA, and DFT studies. All the new compounds showed promising DPPH and Hydroxyl radical scavenging activities, However, two compounds **5g** and **5h** showed excellent activities comparable with standards ascorbic acid and BHA, respectively; which was substantiated by docking and ADMET analysis. Therefore, the compounds **5g** and **5h** can be used as lead antioxidants for further investigations.

Declarations

Author contribution statement

Karthik Kumara: Analyzed and interpreted the data; Wrote the paper.

Malledevarapura Gurumurthy Prabhudeva, Channa Basappa Vagish: Performed the experiments.

Hamse Kameshwar Vivek: Contributed reagents, materials, analysis tools or data.

Kuriya Madavu Lokanatha Rai: Analyzed and interpreted the data.

Neratur Krishnappagowda Lokanath: Conceived and designed the experiments.

Kariyappa Ajay Kumar: Conceived and designed the experiments; Analyzed and interpreted the data; Wrote the paper.

Funding statement

This research did not receive any specific grant from funding agencies in the public, commercial, or not-for-profit sectors.

Data availability statement

Data associated with this study has been deposited at http://www.ccdc.cam.ac.uk/conts/retrieving.html, or from the Cambridge Crystallographic Data Centre, 12 Union Road, Cambridge CB2 1EZ, UK; fax:(+44) 1223-336-033; or e-mail: deposit@ccdc.cam.ac.uk under the accession number CCDC 1838509.

Declaration of interests statement

The authors declare no conflict of interest.

Additional information

No additional information is available for this paper.

Acknowledgements

The authors thanks to the IOE Instrumentation Facility, Vijnana Bhavana, University of Mysore, for recording spectra and X-ray diffraction studies.

References

[1] D. Farbstein, A. Kozak-Blickstein, A.P. Levy, Antioxidant vitamins and their use in preventing cardiovascular disease, Molecules 15 (11) (2010) 8098–8110.
[2] S. Naveen, Karthik Kumara, A. Dileep Kumar, K. Ajay Kumar, A. Zarrouk, I. Warad, N.K. Lokanath, Synthesis, characterization, crystal structure, Hirshfeld surface analysis, antioxidant properties and DFT calculations of a novel pyrazole derivative: ethyl 1-(2,4-dimethylphenyl)-3-methyl-5-phenyl-1H-pyrazole-4-carboxylate, J. Mol. Struct. 1226 (A) (2021) 129350.
[3] J.C. Jeyaveeran, C. Praveen, Y. Arun, A.A.M. Prince, P.T. Perumal, Cycloisomerization of acetylenic oximes and hydrazones under gold catalysis: synthesis and cytotoxic evaluation of isoxazoles and pyrazoles, J. Chem. Sci. 128 (2016) 73–83.
[4] H. Zhang, Q. Wei, G. Zhu, J. Qu, B. Wang, A facile and expeditious approach to substituted 1H-pyrazoles catalyzed by iodine, Tetrahedron Lett. 57 (2016) 2633–2637.
[5] A. Shaabani, H. Sepahvand, M.K. Nejad, A re-engineering approach: synthesis of pyrazolo[1,2-a]pyrazoles and pyrano[2,3-c]pyrazoles via an isocyanide-based four-component reaction under solvent-free conditions, Tetrahedron Lett. 57 (2016) 1435–1437.
[6] A. Dileep Kumar, C.B. Vagish, D.M. Lokeshwari, R. Sowmya, K. Ajay Kumar, Design, synthesis, characterization, evaluation for anticancer and citotoxic properties of new pyrazole carbothioamides, Asian J. Org. & Med. Chem. 6 (1) (2021) 53–58.
[7] P. Fricero, L. Bialy, A.W. Brown, W. Czechtizky, M. Mendez, J.P.A. Harrity, J P A, Synthesis and modular reactivity of pyrazole 5-trifluoroborates: intermediates for the preparation of fully functionalized pyrazoles, J. Org. Chem. 82 (2017) 1688–1696.
[8] D.M. Lokeshwari, V.H. Kameshwar, A.K. Kariyappa, Synthesis of furan tethered 2-pyrazolines via 1,3-dipolar cycloaddition reactions: *In vitro* evaluation for their antioxidant and antimicrobial activities, molecular docking and ADMET studies, Biointerface Res. App. Chem. 7 (5) (2017) 2158–2165.
[9] D.K. Achutha, C.B. Vagish, N. Renuka, D.M. Lokeshwari, A.K. Kariyappa, Green synthesis of novel pyrazoline carbothioamides: a potent antimicrobial and antioxidant agents, Chem. Data Coll. 28 (2020) 100445.
[10] W.K. Vishnu, P. Abeesh, C. Guruvayoorappan, Pyrazole (1, 2-diazole) induce apoptosis in lymphoma cells by targeting BCL-2 and BCL-XL genes and mitigate murine solid tumour development by regulating cyclin-D1 and Ki-67 expression, Toxicol. Appl. Pharmacol. 418 (2021) 115491.
[11] G. Bansal, S. Singh, V. Monga, P.V. Thanikachalam, P. Chawla, Synthesis and biological evaluation of thiazolidine-2,4-dione-pyrazole conjugates as antidiabetic, anti-inflammatory and antioxidant agents, Bioorg. Chem. 92 (2019) 103271.
[12] M.G. Prabhudeva, H.K. Vivek, K. Ajay Kumar, Synthesis of novel pyrazole carboxamides using reusable catalyst as antimicrobial agents and molecular docking studies, Chem. Data Coll. 20 (2019) 100193.
[13] S. Shaikh, P. Dhavan, G. Pavale, M.M.V. Ramana, B.L. Jadhav, Design, synthesis and evaluation of pyrazole bearing α-aminophosphonate derivatives as potential acetylcholinesterase inhibitors against Alzheimer's disease, Bioorg. Chem. 96 (2020) 103589.
[14] H. Zare, Effects of Salvia Officinalis extract on the breast cancer cell line, Sci. Med. J. 1 (1) (2019) 25–29.

[15] O.P. Chzhu, D.E. Araviashvili, I.G. Danilova, Studying properties of prospective biologically active extracts from Marine Hydrobionts, Emerg. Sci. J. 4 (1) (2020) 37–43.
[16] A. Tasneem, G.P. Rai, S. Reyaz, H.R. Bairagya, The possible molecular mechanism of SARS-CoV-2 Main Protease: new structural insights from computational methods, Sci. Med. J. 2 (2020) 108–126 (Sp. Iss. "COVID -19").
[17] C.B. Vagish, A.D. Kumar, K. Kumara, H.K. Vivek, N. Renuka, N.K. Lokanath, K.A. Kumar, Environmentally benign synthesis of substituted pyrazoles as potent antioxidant agents, characterization and docking studies, J. Iran. Chem. Soc. 18 (2021) 479–493.
[18] M. Rana, R. Arif, F.I. Khan, V. Maurya, R. Singh, M.I. Faizan, S. Yasmeen, S.H. Dar, R. Alam, A. Sahu, T. Ahmad, Rahisuddin, Pyrazoline analogs as potential anticancer agents and their apoptosis, molecular docking, MD simulation, DNA binding and antioxidant studies, Bioorg. Chem. 108 (2021) 104665.
[19] R.D. Alharthy, Design and synthesis of novel pyrazolo[3,4-*d*]Pyrimidines: *in vitro* cytotoxic evaluation and free radical scavenging activity studies, Pharm. Chem. J. 54 (2020) 273–278.
[20] L. Liao, J. Shi, C. Jiang, L. Zhang, L. Feng, J. Liu, J. Zhang, Activation of anti-oxidant of curcumin pyrazole derivatives through preservation of mitochondria function and Nrf2 signaling pathway, Neurochem. Int. 125 (2019) 82–90.
[21] H.F. Rizk, M.A. El-Borai, A. Ragab, S.A. Ibrahim, Design, synthesis, biological evaluation and molecular docking study based on novel fused pyrazolothiazole scaffold, J. Iran. Chem. Soc. 17 (2020) 2493–2505.
[22] V. Pogaku, R. Krishnan, S. Basavoju, Synthesis and biological evaluation of new benzo[*d*][1,2,3]triazol-1-yl-pyrazole-based dihydro-[1,2,4]triazolo[4,3-*a*] pyrimidines as potent antidiabetic, anticancer and antioxidant agents, Res. Chem. Intermed. 47 (2021) 551–571.
[23] G. Joshi, M. Sharma, S. Kalra, N.S. Gavande, S. Singh, R. Kumar, Design, synthesis, biological evaluation of 3,5-diaryl-4,5-dihydro-1H-pyrazole carbaldehydes as non-purine xanthine oxidase inhibitors: tracing the anticancer mechanism via xanthine oxidase inhibition, Bioorg. Chem. 107 (2021) 104620.
[24] Rigaku, Crystal Clear, 2011.
[25] G.M. Sheldrick, Shelxt - integrated space-group and crystal-structure determination, Acta Crystallogr. C71 (2015) 3–8.
[26] G.M. Sheldrick, Phase annealing in SHELX-90: direct methods for larger structures, Acta Crystallogr. A46 (1990) 467–473.
[27] A.L. Spek, PLATON, an integrated tool for the analysis of the results of a single crystal structure determination, Acta Crystallogr. A46 (1990) 34.
[28] C.F. Macrae, I.J. Bruno, J.A. Chisholm, P.R. Edgington, P. McCabe, E. Pidcock, L.M. Rodriguez, R. Taylor, J. van de Streek, P.A. Wood, Mercury CSD 2.0-new features for the visualization and investigation of crystal structures, J. Appl. Crystallogr. 41 (2008) 466–470.
[29] G.V. Kumar, M. Govindaraju, N. Renuka, B.B.A. Khatoon, B.N. Mylarappa, K.A. Kumar, Synthesis of 1,3,5-triaryl-4,6-dioxo-pyrrolo[3,4-*d*]-7,8-dihydropyrzoles and their antimicrobial and antioxidant activity, Rasayan J. Chem. 5 (3) (2012) 338–342.
[30] K.R. Raghavendra, N. Renuka, K.A. Kumar, S. Shashikanth, An accessible route for the synthesis of novel lignan derivatives and their biological evaluation, Pharmaceut. Chem. J. 51 (2017) 661–669.
[31] P. Gurunanjappa, V.H. Kameshwar, A.K. Kariyappa, Bioactive formylpyrazole analogues: synthesis, antimicrobial, antioxidant and molecular docking studies, Asian J. Chem. 29 (2017) 1549–1554.
[32] G.M. Sastry, M. Adzhigirey, T. Day, R. Annabhimoju, W. Sherman, Protein and ligand preparation: parameters, protocols, and influence on virtual screening enrichments, J. Comput. Aided Mol. Des. 27 (2013) 221–234.
[33] A. Dileep Kumar, S. Naveen, H.K. Vivek, M. Prabhuswamy, N.K. Lokanath, K. Ajay Kumar, Synthesis, crystal and molecular structure of ethyl 2-(4-chlorobenzylidene)-3-oxobutanoate: studies on antioxidant, antimicrobial activities and molecular docking, Chem. Data Coll. 5 (6) (2016) 36–45.
[34] M.G. Prabhudeva, A.D. Kumara, M.B. Kumar, N.K. Ningappa, K. Lokanath, Ajay Kumar, Amberlyst-15 catalyzed synthesis of novel thiophene–pyrazoline derivatives: spectral and crystallographic characterization and anti-inflammatory and antimicrobial evaluation, Res. Chem. Intermed. 44 (2018) 6453–6468.
[35] A.D. Kumar, M.G. Prabhudeva, S. Bharath, K. Kumara, N.K. Lokanath, K.A. Kumar, Design and Amberlyst-15 mediated synthesis of novel thienyl-pyrazole carboxamides that potently inhibit Phospholipase A2 by binding to an allosteric site on the enzyme, Bioorg. Chem. 80 (2018) 444–452.
[36] A.D. Kumar, H.K. Vivek, B. Srinivasan, S. Naveen, K. Kumara, N.K. Lokanath, K. Byrappa, K.A. Kumar, Design, synthesis, characterization, crystal structure, Hirshfeld surface analysis, DFT calculations, anticancer, angiogenic properties of new pyrazole carboxamide derivatives, J. Mol. Struct. 1235 (2021) 130271.
[37] K. Kumara, A. Dileep Kumar, K. Ajay Kumar, N.K. Lokanath, Synthesis of ethyl 5-(4-chlorophenyl)-3-methyl-1-phenyl-1H-pyrazole-4-carboxylate by an unusual protocol: crystal and molecular structure, Hirshfeld surface analysis, Chem. Data Coll. 9–10 (2017) 89–97.
[38] S.K. Seth, Structural elucidation and contribution of intermolecular interactions in O-hydroxy acyl aromatics: insights from X-ray and Hirshfeld surface analysis, J. Mol. Struct. 1064 (2014) 70–75.
[39] M.A. Spackman, J.J. McKinnon, Fingerprinting intermolecular interactions in molecular crystals, CrystEngComm 4 (66) (2002) 378–392.
[40] J.J. McKinnon, D. Jayatilaka, M.A. Spackman, Towards quantitative analysis of intermolecular interactions with Hirshfeld surfaces, Chem. Commun. (J. Chem. Soc. Sect. D) 37 (2007) 3814–3816.
[41] S.K. Seth, Tuning the formation of MOFs by pH influence: X-ray structural variations and Hirshfeld surface analyses of 2-amino-5-nitropyridine with cadmium chloride, CrystEngComm 15 (2013) 1772–1781.
[42] Y.H. Luo, G.G. Wu, S.L. Mao, B.W. Sun, Complexation of different metals with a novel N-donor bridging receptor and Hirshfeld surfaces analysis, Inorg. Chim. Acta. 397 (2013) 1–9.
[43] J. Bernstein, R.E. Davis, L. Shimoni, N.-L. Chang, Patterns in hydrogen bonding: functionality and graph set analysis in crystals, Angew. Chem., Int. Ed. Engl. 34 (1995) 1555–1573.
[44] K.L. Jyothi, K. Kumara, M.K. Hema, Mahesha, R. Gautam, T.N. Guru Row, N.K. Lokanath, Structural elucidation, theoretical insights and thermal properties of three novel multicomponent molecular forms of gallic acid with hydroxypyridines, J. Mol. Struct. 1207 (2020) 127828.
[45] K. Kumara, K.P. Harish, N. Shivalingegowda, H.C. Tandon, K.N. Mohana, N.K. Lokanath, Crystal structure studies, Hirshfeld surface analysis and DFT calculations of novel 1-[5-(4-methoxy-phenyl)-[1,3,4]oxadiazol-2-yl]-piperazine derivatives, Chem. Data Coll. 11–12 (2017) 40–58.
[46] K. Kumara, A.D. Kumar, K.A. Kumar, N.K. Lokanath, Synthesis, spectral and X-ray crystal structure of 3-(3-methoxyphenyl)-5-(3-methylthiophen-2-yl)-4,5-dihydro-1H-pyrazole-1-carboxamide: Hirshfeld surface, DFT calculations and thermo-optical studies, Chem. Data Coll. 13–14 (2018) 40–59.
[47] K. Kumara, A.D. Kumar, S. Naveen, K.A. Kumar, N.K. Lokanath, Synthesis, spectral characterization and X-ray crystal structure studies of 3-(benzo[d][1,3]dioxol-5-yl)-5-(3-methylthiophen-2-yl)-4,5-dihydro-1*H*-pyrazole-1-carboxamide: Hirshfeld surface, DFT and thermal analysis, J. Mol. Struct. 1161 (2018) 285–298.
[48] S. Xavier, S. Periandy, S. Ramalingam, NBO, conformational, NLO, HOMO–LUMO, NMR and electronic spectral study on 1-phenyl-1-propanol by quantum computational methods, Spectrochim, Acta Part A: Mol. Biomol. Spect. 137 (2015) 306–320.
[49] V.K. Shalini, L. Srinivas, Lipid peroxide induced DNA damage: protection by turmeric (*Curcuma longa)*, Mol. Cell. Biochem. 77 (1987) 3–10, 1987.
[50] C. Kontogiorgis, K.E. Litinas, A. Makri, D.N. Nicolaides, A. Vronteli, D.J. Hadjipavlou-Litina, E. Pontiki, A. Siohou, Synthesis and biological evaluation of novel angular fused pyrrolocoumarins, J. Enzym. Inhib. Med. Chem. 23 (2008) 43–49.
[51] S.A. Ali, S.M. Awad, A.M. Said, S. Mahgoub, H. Taha, N.M. Ahmed, Design, synthesis, molecular modelling and biological evaluation of novel 3-(2-naphthyl)-1-phenyl-1H-pyrazole derivatives as potent antioxidants and 15-Lipoxygenase inhibitors, J. Enzym. Inhib. Med. Chem. 35 (2020) 847–863.
[52] B.P. Bandgar, S.S. Gawande, R.G. Bodade, N.M. Gawande, C.N. Khobragade, Synthesis and biological evaluation of a novel series of pyrazole chalcones as anti-inflammatory, antioxidant and antimicrobial agents, Bioorg. Med. Chem. 17 (2009) 8168–8173.
[53] H. Brahmbhatt, M. Molnar, V. Pavic, Pyrazole nucleus fused tri-substituted imidazole derivatives as antioxidant and antibacterial agents, Karbala Int. J. Modern Sci. 4 (2018) 200–206.
[54] Y. Kaddouri, F. Abrigach, El.B. Yousfi, M. El Kodadi, R. Touzani, New thiazole, pyridine and pyrazole derivatives as antioxidant candidates: synthesis, DFT calculations and molecular docking study, Heliyon 6 (2020), e03185.